### Title

New paleointensity results from rapidly cooled Icelandic lavas: Implications for Arctic geomagnetic field strength




### Journal

Journal of Geophysical Research: Solid Earth, 120(5)

### ISSN

2169-9313



### Authors

Cromwell, G
Tauxe, L
Halldõrsson, SA



### Publication Date

2015-05-01

### DOI

10.1002/2014JB011828

Peer reviewed

AGU PUBLICATIONS

JGR

Journal of Geophysical Research: Solid Earth

RESEARCH ARTICLE

10.1002/2014JB011828

**Key Points:**
- Forty-four new paleointensity results from Iceland for 0–3.5 Ma
- Iceland intensity agrees with long-term dipole moment estimates of 42 ZAm2
- Recalculated Antarctic intensity similar to Arctic results

**Correspondence to:**
G. Cromwell,
cromwell@oxy.edu

**Citation:**
Cromwell, G., L. Tauxe, and S. A. Halldórsson (2015), New paleointensity results from rapidly cooled Icelandic lavas: Implications for Arctic geomagnetic field strength, *J. Geophys. Res. Solid Earth*, *120*, 2913–2934, doi:10.1002/2014JB011828.

Received 8 DEC 2014
Accepted 22 APR 2015
Accepted article online 6 MAY 2015
Published online 30 MAY 2015

# New paleointensity results from rapidly cooled Icelandic lavas: Implications for Arctic geomagnetic field strength

**G. Cromwell[1,2], L. Tauxe[1], and S. A. Halldórsson[1,3]**

[1]Geosciences Research Division, Scripps Institution of Oceanography, University of California, San Diego, La Jolla, California, USA, [2]Now at Department of Geology, Occidental College, Los Angeles, California, USA, [3]Now at Nordic Volcanological Centre, Institute of Earth Sciences, University of Iceland, Reykjavík, Iceland

**Abstract** The Earth's magnetic field is assumed to be a geocentric axial dipole (GAD) when averaged over sufficient time ($10^5$–$10^6$ years). Recent investigations of global paleosecular variation and time-averaged field behavior on million year timescales generally support a predominantly dipole field in the Northern Hemisphere, but unique field structures at high southern latitudes suggest the presence of a substantial $\bar{g}_2^0$ quadrupolar component. Average paleointensity results from Antarctica are approximately half the value predicted by a GAD field; this behavior has not been sufficiently investigated because there is a paucity of absolute paleointensity data from the high latitudes of the Arctic and Antarctic, so no adequate comparisons have been made between the two regions. We collected glassy volcanic material from 129 subaerial and subglacial volcanic units in Iceland in order to provide a suitable intensity data set at high northern latitudes. Forty-four sites met our very strict specimen and site level selection criteria. Four Holocene sites have a median intensity value of 55.8 ± 15.6 μT (virtual axial dipole moment = 78.1 ± 22.0 ZAm$^2$), consistent with the present-day field. Thirty-seven sites are between 11 ka and 3.35 Ma with a median intensity of 33.1 ± 8.3 μT (47.0 ± 11.6 ZAm$^2$). This median intensity is indistinguishable from some long-term global field strength estimates. Reevaluation of existing high-latitude data suggests a general agreement with our Iceland results, but there are still too few Antarctic sites to adequately compare Arctic and Antarctic field behaviors.

## 1. Introduction

The Earth's ancient magnetic field can be approximated by a geocentric axial dipole (GAD) in which the average field intensity is twice as strong at the poles as it is at the equator. The present-day geomagnetic field and the Holocene time-averaged field [e.g., *Korte et al.*, 2011] generally support the GAD hypothesis with a virtual axial dipole moment (VADM) of about 80 ZAm$^2$ but both also suggest some hemispheric asymmetry in the average field. A VADM of 80 ZAm$^2$ corresponds to surface field intensities of ~30 μT and 60 μT at the equator and poles, respectively (red line in Figure 1).

In a departure from the long-standing belief that the present field strength is representative of the long-term average [e.g., *Tanaka et al.*, 1995a], *Juarez et al.* [1998] suggested that the long-term average field (5–160 Ma) was ~42 ZAm$^2$ (supported more recently by *Tauxe et al.* [2013] for 0–140 Ma), implying equatorial and polar fields of ~16 μT and ~32 μT, respectively (blue dashed line in Figure 1). In line with this prediction, *Lawrence et al.* [2009] found an average field of 31.5 ± 2.4 μT in Antarctica (0–6.7 Ma), similar to the predictions of *Juarez et al.* [1998] and *Tauxe et al.* [2013] (compare blue dashed line with ~80°S bin in Figure 1).

In contrast to the decidedly non-GAD behavior in the published intensity data shown in Figure 1 (where each latitude bin may or may not be representative of the time-averaged field), directional data, in particular, inclinations, are much more consistent with a GAD field with only small contributions from non-GAD components required to fit the data for the last few million years [e.g., *Kelly and Gubbins*, 1997; *Johnson and Constable*, 1996; *Glatzmaier et al.*, 1999]. An explanation for the paleointensity departures from GAD is geodynamic differences in the outer core [e.g., *Olson and Aurnou*, 1999; *Jackson et al.*, 2000; *Hulot et al.*, 2002; *Gubbins et al.*, 2006] expressed as maximum and minimum flux zones within the tangent cylinder [e.g., *Christensen et al.*, 1998]. Some time-averaged field models such as CALS10k.1b [*Korte et al.*, 2011], GUFM1 [*Jackson et al.*, 2000], and paleosecular variation (PSV) studies [e.g., *Johnson and Constable*, 1996] observe unusual field structures at high latitudes, notably the presence of persistent flux lobes in both the Arctic and Antarctic regions.

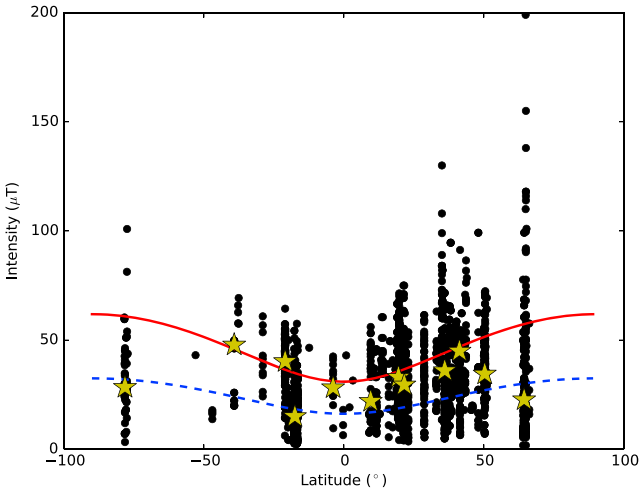


**Figure 1.** Site level paleointensity data (method code of LP-PI-TRM), with standard deviations ≤15% or ≤5 μT downloaded from the MagIC database (http://earthref.org/MagIC) from the last 5 Myr. Data are plotted against latitude, and median values for 10° bins are shown as yellow stars. Predicted values for dipole moments of 80 $ZAm^2$ (present field) and 42 $ZAm^2$ [*Juarez et al.*, 1998; *Tauxe et al.*, 2013] are shown as solid red and dashed blue lines, respectively.

A comparison of Arctic and Antarctic paleointensity results over similar timescales (0–5 Ma) might offer insights into the long-term behavior of the geomagnetic field at high latitudes.

Figure 1 shows that there are many paleointensity results from high northern latitudes. The majority of these studies have been conducted in Iceland, which is located just below the Arctic circle. As a result of ~15 Myr [*McDougall et al.*, 1984] of continuous volcanism, Iceland contains an abundance of well-exposed subaerial and subglacial volcanic sequences. Major objectives of most paleomagnetic studies in Iceland have been to provide magnetostratigraphic controls for local geologic formations [e.g., *Walker*, 1959; *Watkins and Walker*, 1977; *McDougall et al.*, 1984; *Kristjánsson et al.*, 1998; *Helgason and Duncan*, 2001; *Kristjánsson*, 2010], evaluate secular variation of the ancient geomagnetic field [e.g., *Tanaka et al.*, 1995b; *Udagawa et al.*, 1999; *Kristjánsson*, 2013], and define the characteristics of geomagnetic reversals [e.g., *Shaw*, 1975; *Kristjánsson et al.*, 1980; *Goguitchaichvili et al.*, 1999] or excursions [e.g., *Marshall et al.*, 1988; *Levi et al.*, 1990; *Camps et al.*, 2011; *Jicha et al.*, 2011]. Paleointensity studies in Iceland have focused primarily on transitional field events [e.g., *Lawley*, 1970; *Shaw*, 1975; *Marshall et al.*, 1988; *Goguitchaichvili et al.*, 1999; *Brown et al.*, 2006; *Ferk and Leonhardt*, 2009], while relatively little work has been done to explore the strength of the magnetic field during stable polarity intervals, which is necessary for investigations of long-term geomagnetic field behavior.

Several Icelandic studies do provide intensity results that are potentially useful for Arctic/Antarctic comparisons [e.g., *Schweitzer and Soffel*, 1980; *Senanayake et al.*, 1982; *Roberts and Shaw*, 1984; *Tanaka et al.*, 1995a; *Stanton et al.*, 2011; *Tanaka et al.*, 2012]. However, such investigations are dependent on the ability of lava flows to accurately record magnetic field strength. *Love and Constable* [2003], *Herrero-Bervera and Valet* [2009], and *Cromwell et al.* [2015] compiled results from the 1960 Kilauea lava flow on the Big Island of Hawaii and found that the majority of published paleointensity estimates of the flow do not consistently recover the expected field strength. *Love and Constable* [2003] estimated that available data from the 1960 flow had a 19% standard deviation of the mean and an average field strength of 33.91 μT (expected field = 36.0 μT). Different experimental techniques and selection criteria contribute to the variance in the Kilauea data, and *Cromwell et al.* [2015] suggested that a major cause of erroneous field estimates is the type of volcanic material used in laboratory experiments.

Most paleointensity studies collect samples from the slowly cooled, massive interiors of lava flows. These samples have relatively large crystals and often produce large ($\gtrsim$ 200 nm), multidomain magnetic grains. It is common for multidomain specimens to yield curved, concave-up Arai plots [*Dunlop and Özdemir*, 2001] during paleointensity experiments, frequently resulting in subjective natural remanent magnetization/thermal remanent magnetization (NRM/TRM) slope interpretations. Multidomain paleointensity results are also shown to consistently underestimate expected magnetic field strength when calculated using the full thermal remanent magnetization (TRM) [*Cromwell et al.*, 2013, 2015]. Single-domain magnetic grains, on the other hand, are significantly smaller ($\lesssim$ 80 nm) and are expected to respond well to paleomagnetic experiments. Distributions of single-domain particles can be found in most volcanic rock types, but they comprise an especially large percentage of volcanic glasses and other quenched materials. Terrestrial and submarine volcanic glass has been used for paleointensity investigations of the ancient magnetic field [e.g., *Pick and Tauxe*, 1993a; *Kent and Gee*, 1996; *Tauxe and Staudigel*, 2004; *Bowles et al.*, 2006; *Ferk and Leonhardt*, 2009; *Ferk et al.*, 2011; *Tauxe et al.*, 2013], and recently, *Cromwell et al.* [2015] showed that rapidly cooled material from subaerially erupted

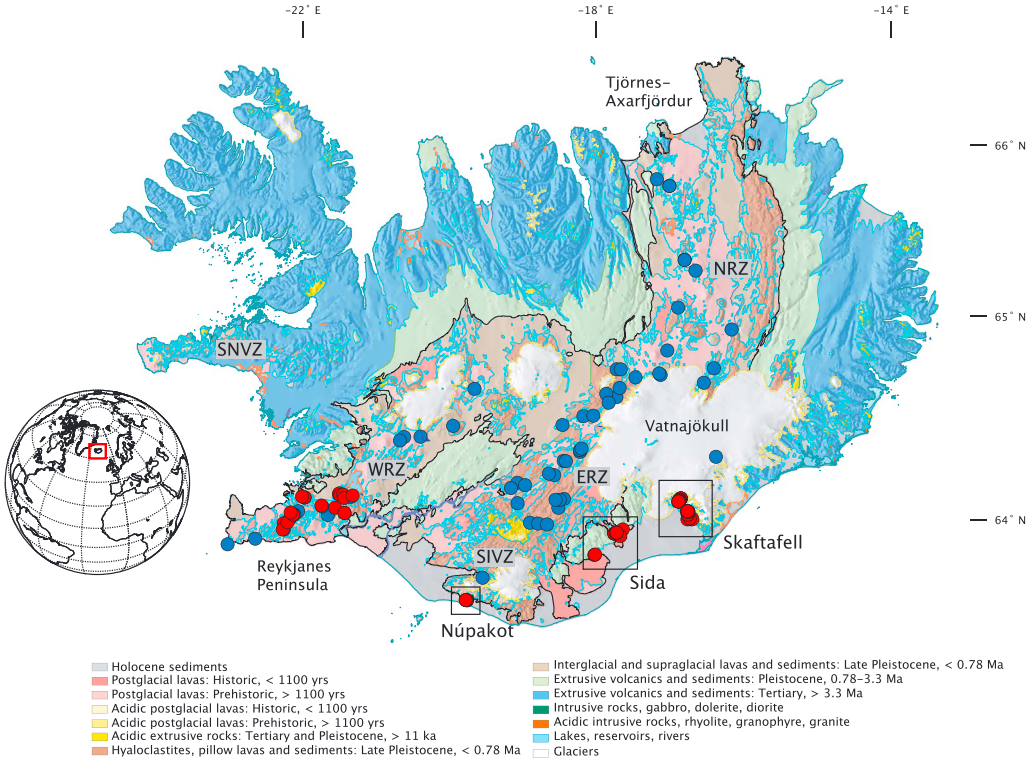


**Figure 2.** Geologic map of Iceland showing regional volcanic systems. The Western (WRZ), Eastern (ERZ), and Northern (NRZ) axial rift zones are labeled, as well as the off-axis South Iceland (SIVZ) and Snaefellsness (SNVZ) volcanic zones. The neovolcanic zone (<780 ka) is outlined in black and is our largest sampling region. Núpakot, Sida, and Skaftafell are sampling areas specific to the 2012 field expedition, comprising geologic formations older than 780 ka. Site locations from the pre-2006 and 2008 field seasons are plotted in blue ($N = 63$) and the 2012 sites are in red ($N = 66$). Geology derived from *Jóhannesson and Saemundsson* [2009] and the Icelandic Institute of Natural History.

Hawaiian lavas can consistently recover the expected field strength. The success of glassy, rapidly cooled material in paleointensity experiments makes it ideal for global investigations of the ancient geomagnetic field when it has persisted in a near-pristine state and has not altered or devitrified over time. Iceland is an excellent study location for this purpose due to the accessibility of subglacial volcanic sequences emplaced during the last ~3 Ma [*McDougall et al.*, 1977; *Helgason and Duncan*, 2001] and possibly as far back as late Miocene time [*Geirsdóttir and Eiríksson*, 1994].

In this study we present a new collection of Icelandic volcanic glasses from subglacial and subaerial lava flows in order to evaluate the paleointensity in Iceland over the last few million years. We apply strict selection criteria to ensure an accurate representation of field strength and then compare our results to current field models and published high-latitude data that pass our selection criteria. Here we discuss the time-averaged strength of the geomagnetic field in the Arctic and the possibility of long-term hemispheric asymmetry at high latitudes.

## 2. Geologic Setting

Iceland is a volcanic island situated on the Mid-Atlantic Ridge at the boundary between the North American and Eurasian Plates (Figure 2). Iceland has an unusually thick crust due to a high degree of melting associated with a mantle hot spot beneath the island [*Bjarnason and Schmeling*, 2009]. Constant spreading between the North American and Eurasian plates means that the oldest rocks in Iceland, ~15 Ma [*McDougall et al.*, 1984], are found in the eastern and westernmost parts of the island, with progressively younger formations generally occurring closer to the spreading axis. Active volcanism occurs in the neovolcanic zone (0–0.78 Ma) which transects the length of the island from the Reykjanes Peninsula in the southwest to the Tjörnes-Axarfjördur region in the northeast (Figure 2). The neovolcanic zone is differentiated between an axial rift zone and off-rift volcanic zones. The axial rift zone spans the length of Iceland and is divided into Western (WRZ), Eastern (ERZ),

and Northern (NRZ) rift zone segments (Figure 2). Two off-rift volcanic zones are the South Iceland Volcanic Zone (SIVZ), an extension of the ERZ, and the Snaefellsnes Volcanic Zone (SNVZ), which is an intraplate volcanic system and not directly related to active plate boundary volcanism [*Einarsson*, 2008].

## 3. Sample Collection

Glassy and rapidly cooled fine-grained volcanic material was collected over several field seasons (pre-2006, 2008, and 2012) for isotope geochemistry and paleomagnetic analysis. Early field expeditions were initially organized by the University of Iceland and later by Dr. David Hilton's research group at Scripps Institution of Oceanography (SIO) and the University of Iceland as part of an ongoing project directed at the volatile characteristics of the Iceland mantle plume [*Macpherson et al.*, 2005; *Füri et al.*, 2010; *Barry et al.*, 2014]. Fresh glassy material from these expeditions were collected from subglacial volcanic units throughout the neovolcanic zone. The 2012 field season was organized by the paleomagnetic group at SIO with the goal of adding to the existing collection of Brunhes age (0–0.78 Ma), neovolcanic glasses and by targeting subglacial units with a greater age range (0–4 Ma) in the Núpakot, Sida, and Skaftafell areas (Figure 2). The 2012 sampling plan was guided by previous work on subglacial and subaerial volcanic sequences, including *Kristjánsson et al.* [1980, 1988], *Bergh and Sigvaldason* [1991], *Helgason and Duncan* [2001], *Füri et al.* [2010], and *Stanton et al.* [2011]. All sites are listed in Table 1 along with their correlated formation names, available age estimates, and location information.

### 3.1. Neovolcanic Zone

The neovolcanic zone contains formations emplaced during the Brunhes chron (0–0.78 Ma). Most geologic formations in the neovolcanic zone are stratigraphically constrained using geologic maps [e.g., *Jóhannesson and Saemundsson*, 2009; *Saemundsson et al.*, 2010] and have relatively large age uncertainties. Absolute geochronology is rare because Icelandic basalts (the dominant rock type formed in the last 0.78 Ma) have low potassium content [e.g., *Jakobsson et al.*, 2008] which makes age estimates from traditional $^{40}K/^{39}Ar$ and $^{40}Ar/^{39}Ar$ methods difficult to acquire. $^{14}C$ radiometric dates are available [e.g., *Jónsson*, 1974; *Hjartarson*, 1994; *Sinton et al.*, 2005], but the absolute range of this method is limited to ~50 ka. The majority of published $^{40}K/^{39}Ar$ and $^{40}Ar/^{39}Ar$ dates in Iceland are from units significantly older than 0.78 Ma [e.g., *Saemundsson and Noll*, 1974; *McDougall et al.*, 1977, 1984; *Helgason and Duncan*, 2001], while only a few radiometric ages are available for lavas younger than 0.78 Ma [e.g., *Levi et al.*, 1990; *Jicha et al.*, 2011]. Recent work by *Guillou et al.* [2010] suggests that an unspiked K-Ar method can successfully date Quaternary Icelandic lavas and potentially be used to constrain the ages of volcanic units emplaced between the reliability timescales of $^{14}C$ and traditional K-Ar series geochronology.

In general, neovolcanic geology is divided into a postglacial period (< 11 ka, Holocene) dominated by subaerial lava flows (e.g., Figures 3c and 3d) and an older period of subglacial or interglacial (11–780 ka, Brunhes) pillow basalts (Figure 3a), hyaloclastite sequences (Figure 3b), or interglacial lava flows [*Jóhannesson and Saemundsson*, 2009]. Samples collected on the Reykjanes Peninsula have better age control than those in the ERZ and NRZ due to a greater level of detail of available geologic maps in southwest Iceland compared to other parts of the country. *Saemundsson et al.* [2010] subdivide the Reykjanes Peninsula into postglacial historic (0–1.3 ka) and prehistoric (1.3–11 ka) lavas, and Late Weichsel (11-21 ka) subglacial lavas, Early Weichsel (21-110 ka) subglacial lavas, and Early Brunhes (110–780 ka) volcanic units. The Weichsel period encompasses the last glaciation from approximately 11–110 ka, and peak glaciation at 21 ka separates the "Late" and "Early" periods.

In total, we sampled 80 distinct volcanic units from the neovolcanic zone. Sixty-one units were collected before 2008, and 19 units were collected during the 2012 field season. Four Weichsel lavas from the 2006–2008 collection (KLE-1, NES-2, OLF-1, and SKARD-1) were resampled in 2012 to supplement the limited amount of material. All samples from these units are combined into the 2012 naming convention (isl004 and isl011–isl013, respectively).

### 3.2. Núpakot

The Núpakot sampling area is located on the southern flank of the Eyjafjöll volcanic system in the SIVZ (Figure 2) and is composed of interglacial lavas and subglacial hyaloclastite layers. *Jóhannesson* [1985] identified the Brunhes/Matuyama (B/M) polarity transition in a sequence of lavas near the Núpakot farm. Magnetostratigraphy by *Kristjánsson et al.* [1988] located the polarity transition approximately 50 m above the base of this outcrop (section A; all section and flow names referenced here are from *Kristjánsson et al.* [1988]),

AGU Journal of Geophysical Research: Solid Earth

10.1002/2014JB011828

**Table 1.** Average Paleointensity Results and Location Information for All Iceland Sites[a]

| Site | Alternative Name | Region | Location | Latitude (°N) | Longitude (°E) | Sample Type | Age | Age Reference | *nn* | $B_F$ | $B_{F\sigma}$ | $B_{F\sigma}$ (%) | VADM | $VADM_\sigma$ |
|---|---|---|---|---|---|---|---|---|---|---|---|---|---|---|
| isl001 | | WRZ | Draugahlidar | 64.05337 | −21.53227 | Pillow margin | Early Weichsel | *Saemundsson et al.* [2010] | | | | | | |
| isl002 | | WRZ | Stakur | 63.99739 | −21.88661 | Pillow margin | Early Weichsel | *Saemundsson et al.* [2010] | 12 | 40.41 | 2.95 | 7.29 | 5.65E+22 | 4.12E+21 |
| isl003 | | WRZ | Nordlingaháls | 63.94583 | −22.00179 | Hyaloclastite | Early Weichsel | *Saemundsson et al.* [2010] | | | | | | |
| isl004 | KLE-1[b,c] | WRZ | Kleifarvatn | 63.91118 | −22.01106 | Pillow margin | Late Weichsel | *Saemundsson et al.* [2010] | | | | | | |
| isl005 | | WRZ | Blesaflöt | 63.95283 | −21.95390 | Flow top | Early Brunhes | *Saemundsson et al.* [2010] | | | | | | |
| isl006 | | WRZ | Stakur | 63.99659 | −21.88837 | Pillow margin | Early Weichsel | *Saemundsson et al.* [2010] | Results combined with isl002 | | | | | |
| isl007 | | WRZ | Dyrafjöll | 64.12054 | −21.31619 | Hyaloclastite | Late Weichsel | *Saemundsson et al.* [2010] | 5 | 17.51 | 0.65 | 3.73 | 2.45E+22 | 9.08E+20 |
| isl008 | | WRZ | Dyrafjöll | 64.12514 | −21.30965 | Hyaloclastite | Early Weichsel | *Saemundsson et al.* [2010] | | | | | | |
| isl009 | | WRZ | Dyrafjöll | 64.11542 | −21.29806 | Hyaloclastite | Early Weichsel | *Saemundsson et al.* [2010] | 5 | 17.2 | 1.5 | 8.5 | 2.40E+22 | 2.10E+21 |
| isl010 | | WRZ | Nesjavellir | 64.11833 | −21.26096 | Agglutinate | < 2 ka | *Saemundsson et al.* [2010] | 4 | 83.88 | 6.49 | 7.73 | 1.17E+23 | 9.06E+21 |
| isl011 | NES-1[b,c] | WRZ | Nesjavellir | 64.10016 | −21.24725 | Pillow margin | Late Weichsel | *Saemundsson et al.* [2010] | 10 | 26.53 | 2.54 | 9.56 | 3.71E+22 | 3.55E+21 |
| isl012 | OLF-1[b,c] | WRZ | Ölfusvatnsfjöll | 64.11546 | −21.14066 | Pillow margin | Early Weichsel | *Saemundsson et al.* [2010] | 6 | 35.04 | 3.28 | 9.36 | 4.89E+22 | 4.58E+21 |
| isl013 | SKARD-1[b,c] | WRZ | Skardsmýrarfjall | 64.04375 | −21.35805 | Pillow margin | Late Weichsel | *Saemundsson et al.* [2010] | 14 | 41.15 | 2.86 | 6.96 | 5.75E+22 | 4.00E+21 |
| isl014 | | WRZ | Hverakjálki | 64.01681 | −21.23582 | Hyaloclastite | Early Brunhes | *Saemundsson et al.* [2010] | | | | | | |
| isl014b | | WRZ | Hverakjálki | 64.01681 | −21.23582 | Crystalline flow | Early Brunhes | *Saemundsson et al.* [2010] | 3 | 61.98 | 4.99 | 8.06 | 8.66E+22 | 6.97E+21 |
| isl015 | SV13[d] | Skaftafell | Svinafell | 63.98347 | −16.84140 | Pillow margin/ dike margin | > 0.757 Ma | *Helgason and Duncan* [2001] | | | | | | |
| isl016 | SV14[d] | Skaftafell | Svinafell | 63.98148 | −16.83116 | Dike margin | > 0.757 Ma | *Helgason and Duncan* [2001] | | | | | | |
| isl017 | SV14[d] | Skaftafell | Svinafell | 63.98148 | −16.83116 | Lava flow bottom | > 0.757 Ma | *Helgason and Duncan* [2001] | | | | | | |
| isl018 | SV21[d] | Skaftafell | Svinafell | 63.98137 | −16.87985 | Flow bottom and hyaloclastite | 0.65 Ma | *Helgason and Duncan* [2001] | | | | | | |
| isl019 | SV23[d] | Skaftafell | Svinafell | 63.98146 | −16.81626 | Pillow margin and flow top | < 0.65 Ma | *Helgason and Duncan* [2001] | | | | | | |
| isl020 | SV12[d] | Skaftafell | Svinafell | 63.98666 | −16.84952 | Pillow margin | < 0.780 Ma | *Helgason and Duncan* [2001] | 6 | 30.94 | 0.72 | 2.34 | 4.33E+22 | 1.01E+21 |
| isl021 | | Skaftafell | Skaftafellsfjöll | 64.09930 | −16.95398 | Dike margin | | | | | | | | |
| isl022 | | Skaftafell | Skaftafellsfjöll | 64.09930 | −16.95398 | Dike margin | | | | | | | | |
| isl023 | JM10[d] | Skaftafell | Skaftafellsfjöll | 64.09930 | −16.95398 | Hyaloclastite | Matuyama | *Helgason and Duncan* [2001] | | | | | | |
| isl024 | JM10[d] | Skaftafell | Skaftafellsfjöll | 64.09921 | −16.95598 | Pillow margin | Matuyama | *Helgason and Duncan* [2001] | | | | | | |
| isl025 | | Skaftafell | Skaftafellsfjöll | 64.09046 | −16.96967 | Dike margin | | | | | | | | |
| isl026 | JM8A[d] | Skaftafell | Skaftafellsfjöll | 64.09050 | −16.96996 | Hyaloclastite | Matuyama/ Gauss | *Helgason and Duncan* [2001] | | | | | | |
| isl027 | JM8C[d] | Skaftafell | Skaftafellsfjöll | 64.09065 | −16.97126 | Flow bottom | Lower Matuyama | *Helgason and Duncan* [2001] | | | | | | |
| isl028 | JM8C[d] | Skaftafell | Skaftafellsfjöll | 64.09040 | −16.97148 | Hyaloclastite | Lower Matuyama | *Helgason and Duncan* [2001] | | | | | | |
| isl029 | | Skaftafell | Skaftafellsfjöll | 64.09040 | −16.97148 | Dike margin | | | | | | | | |
| isl030 | | Skaftafell | Skaftafellsfjöll | 64.09200 | −16.97715 | Dike margin | | | | | | | | |

Journal of Geophysical Research: Solid Earth

10.1002/2014JB011828

**Table 1.** (continued)

| Site | Alternative Name | Region | Location | Latitude (°N) | Longitude (°E) | Sample Type | Age | Age Reference | *nn* | $B_F$ | $B_{F\sigma}$ | $B_{F\sigma}$ (%) | VADM | VADM$_\sigma$ |
|---|---|---|---|---|---|---|---|---|---|---|---|---|---|---|
| isl031 | | Skaftafell | Skaftafellsfjöll | 64.09194 | −16.97571 | Dike margin | | | | | | | | |
| isl032 | JM7B[d] | Skaftafell | Skaftafellsfjöll | 64.08807 | −16.97369 | Hyaloclastite | Upper Gauss | *Helgason and Duncan* [2001] | | | | | | |
| isl033 | | Skaftafell | Skaftafellsfjöll | 64.08343 | −16.98093 | Dike margin | | | | | | | | |
| isl034 | JM6[d] | Skaftafell | Skaftafellsfjöll | 64.08201 | −16.98469 | Pillow margin | Upper Gauss | *Helgason and Duncan* [2001] | | | | | | |
| isl035 | JM7B[d] | Skaftafell | Skaftafellsfjöll | 64.08288 | −16.98726 | Pillow fragments | Upper Gauss | *Helgason and Duncan* [2001] | | | | | | |
| isl036 | | Skaftafell | Skaftafellsfjöll | 64.08248 | −16.98587 | Pillow margin | | | | | | | | |
| isl037 | HM0 (?)[d] | Skaftafell | Hafrafell | 64.00855 | −16.87314 | Flow bottom | > 3.94 ± 0.06 Ma | *Helgason and Duncan* [2001] | | | | | | |
| isl038 | HM1 (?)[d] | Skaftafell | Hafrafell | 64.00810 | −16.87360 | Pahoehoe flow top | 3.94 ± 0.06 Ma | *Helgason and Duncan* [2001] | | | | | | |
| isl039 | HM1 (?)[d] | Skaftafell | Hafrafell | 64.00810 | −16.87360 | Thin flow | 3.94 ± 0.06 Ma | *Helgason and Duncan* [2001] | | | | | | |
| isl040 | HM3[d] | Skaftafell | Hafrafell | 64.02699 | −16.88276 | Hyaloclastite | 3.20–3.94 Ma | *Helgason and Duncan* [2001] | | | | | | |
| isl041 | HM7[d] | Skaftafell | Hafrafell | 64.02683 | −16.88011 | Flow top | 3.2–3.35 Ma | *Helgason and Duncan* [2001] | 3 | 46.93 | 3.61 | 7.7 | 6.56E+22 | 5.05E+21 |
| isl042 | HM15[d] | Skaftafell | Hafrafell | 64.02672 | −16.87772 | Flow margin | 1.69–2.35 Ma | *Helgason and Duncan* [2001] | | | | | | |
| isl043 | HM31[d] | Skaftafell | Hafrafell | 64.02198 | −16.86354 | Poor pillow margin | 1.69 ± 0.29 Ma | *Helgason and Duncan* [2001] | | | | | | |
| isl044 | HM31[d] | Skaftafell | Hafrafell | 64.02224 | −16.86370 | Pillow fragments | 1.69 ± 0.29 Ma | *Helgason and Duncan* [2001] | | | | | | |
| isl045 | HM11[d] | Skaftafell | Hafrafell | 64.02675 | −16.87363 | Flow margin | 2.35–2.59 Ma | *Helgason and Duncan* [2001] | 4 | 47.06 | 4.38 | 9.3 | 6.58E+22 | 6.12E+21 |
| isl046 | HM8[d] | Skaftafell | Hafrafell | 64.02644 | −16.87453 | Sill margin | 3.20 ± 0.09 Ma | *Helgason and Duncan* [2001] | | | | | | |
| isl047 | | Sida | Kálfafell | 63.93560 | −17.70288 | Flow top | 5.194 ± 0.04 ka | *Höskuldsson et al.* [2012] | 6 | 66.48 | 4.87 | 7.32 | 9.30E+22 | 6.81E+21 |
| isl048 | Laki[e], RH10[f] | Sida | Eldvatnstangi | 63.89852 | −17.73606 | Pahoehoe flow top | 1783 C.E. | *Thordarson and Hoskuldsson* [2008] | 13 | 45.12 | 2.5 | 5.54 | 6.31E+22 | 3.50E+21 |
| isl049 | | Sida | Landbrotshólar | 63.76461 | −17.95491 | Glassy agglutinate | 934 C.E. | *Thordarson and Hoskuldsson* [2008] | | | | | | |
| isl050 | BS3[g] | Sida | Merkurheidi | 63.79651 | −18.06877 | Hyaloclastite | 2.58 Ma | *Saemundsson and Jóhannesson* [1980] | | | | | | |
| isl051 | BS2[g] | Sida | Seljalandsheidi | 63.91316 | −17.81171 | Pillow margin | 2.58 Ma | *Saemundsson and Jóhannesson* [1980] | 6 | 20.56 | 1.2 | 5.83 | 2.88E+22 | 1.68E+21 |
| isl052 | isl048[b] | Sida | Seljalandsheidi | 63.91256 | −17.81103 | Glassy flow top | 1783 C.E. | *Thordarson and Hoskuldsson* [2008] | Results combined with isl048 | | | | | |
| isl053 | BS5[g] | Sida | Seljalandsheidi | 63.91739 | −17.78941 | Altered pillow breccia | 2.58 Ma | *Saemundsson and Jóhannesson* [1980] | | | | | | |
| isl054 | BS9[g] | Sida | Seljalandsheidi | 63.91735 | −17.79268 | Pillow breccia | 2.58 Ma | *Saemundsson and Jóhannesson* [1980] | 6 | 32.82 | 1.29 | 3.94 | 4.59E+22 | 1.80E+21 |
| isl055 | BS5[g] | Sida | Seljalandsheidi | 63.91885 | −17.78666 | Pillow fragment | 2.58 Ma | *Saemundsson and Jóhannesson* [1980] | | | | | | |
| isl056 | BS5[g] | Sida | Seljalandsheidi | 63.91736 | −17.78472 | Hyaloclastite | 2.58 Ma | *Saemundsson and Jóhannesson* [1980] | | | | | | |
| isl057 | | Sida | Seljalandsheidi | 63.91763 | −17.78318 | Dike margin | 2.58 Ma | *Saemundsson and Jóhannesson* [1980] | 5 | 23.39 | 0.63 | 2.69 | 3.27E+22 | 8.81E+20 |
| isl058 | BS5[g] | Sida | Seljalandsheidi | 63.91775 | −17.78188 | Pillow margin | 2.58 Ma | *Saemundsson and Jóhannesson* [1980] | 3 | 24.57 | 0.05 | 0.19 | 3.44E+22 | 6.99E+19 |
| isl059 | | Nupakot | Nupakot Farm | 63.54620 | −19.66770 | Dike margin | ~0.78 Ma | *Kristjánsson et al.* [1988] | | | | | | |
| isl060 | | Nupakot | Nupakot Farm | 63.54607 | −19.66775 | Lava flow bottom | ~0.78 Ma | *Kristjánsson et al.* [1988] | | | | | | |
| isl061 | | Nupakot | Farm by Nupakot | 63.54724 | −19.68457 | Dike margin | ~0.78 Ma | *Kristjánsson et al.* [1988] | | | | | | |
| isl062 | | Nupakot | Farm by Nupakot | 63.54698 | −19.68522 | Hyaloclastite | ~0.78 Ma | *Kristjánsson et al.* [1988] | | | | | | |

**Table 1.** (continued)

| Site | Alternative Name | Region | Location | Latitude (°N) | Longitude (°E) | Sample Type | Age | Age Reference | *nn* | $B_F$ | $B_{F\sigma}$ | $B_{F\sigma}$ (%) | VADM | VADM$_\sigma$ |
|---|---|---|---|---|---|---|---|---|---|---|---|---|---|---|
| isl063 | BS1[g] | Sida | Merkurheidi | 63.79868 | −18.05797 | Hyaloclastite | 2.58 Ma | *Saemundsson and Jóhannesson* [1980] | 3 | 50.58 | 1.32 | 2.61 | 7.08E+22 | 1.85E+21 |
| isl064 | Leit.[e], RH01[e] | WRZ | Raudholar | 64.09447 | −21.75119 | Agglutinate | 5.254 ± 0.206 ka | *Sinton et al.* [2005] | | | | | | |
| isl065 | | WRZ | Raudholar | 64.09514 | −21.75180 | Flow top | 7–11 ka | *Saemundsson et al.* [2010] | 7 | 59.66 | 2.04 | 3.42 | 8.33E+22 | 2.85E+21 |
| isl066 | Kap.[e] | WRZ | Háibruni | 64.00761 | −21.92108 | Flow bottom | 0.799 ka | *Jóhannesson and Einarsson* [1988] | | | | | | |
| isl067 | | WRZ | Bugda | 64.09901 | −21.78453 | Pillow margin | Early Brunhes | *Saemundsson et al.* [2010] | | | | | | |
| A2 | | WRZ | Thórólfsfell | 64.44878 | −20.51725 | Pillow margin | Weichsel | This study | | | | | | |
| A3 | | WRZ | Hödufell | 64.42900 | −20.57036 | Pillow margin | Late Weichsel | *Licciardi et al.* [2007] | | | | | | |
| A4 | | WRZ | Fagradalsfjöll-1 | 64.45283 | −20.30611 | Pillow margin | Late Weichsel | *Licciardi et al.* [2007] | | | | | | |
| A6 | | WRZ | Bláfjall | 64.51564 | −19.88783 | Pillow margin | Saale | This study | | | | | | |
| A8 | | WRZ | Thverbrekknamúli-2 | 64.72322 | −19.61464 | Pillow margin | Weichsel | This study | 5 | 78.45 | 2.22 | 2.83 | 1.09E+23 | 3.09E+21 |
| A11 | | ERZ | Hnottóttaalda | 64.52200 | −18.47167 | Pillow margin | Weichsel | This study | | | | | | |
| A15 | ICE08R-11[b,c] | ERZ | Vatnsfellsvirkjun | 64.20183 | −19.05564 | Pillow margin | Weichsel | This study | 7 | 19.03 | 0.73 | 3.83 | 2.66E+22 | 1.02E+21 |
| A24 | | ERZ | Mid-Bálkafell | 64.67300 | −17.76611 | Pillow margin | Weichsel | This study | 4 | 62.19 | 5.03 | 8.09 | 8.66E+22 | 7.00E+21 |
| A26 | | ERZ | Vonarskard | 64.69231 | −17.89653 | Pillow margin | Weichsel | This study | 3 | 40.1 | 2.83 | 7.05 | 5.58E+22 | 3.94E+21 |
| A27 | | ERZ | Kirkjufellsvatn | 63.97903 | −18.89628 | Pillow margin | | | | | | | | |
| A28 | | ERZ | Klappagil | 63.97414 | −18.79219 | Pillow margin | Weichsel | This study | 4 | 31.19 | 1.87 | 5.98 | 4.36E+22 | 2.61E+21 |
| A29 | | ERZ | Hördufell | 63.96903 | −18.67975 | Pillow margin | Weichsel | This study | | | | | | |
| A30 | | ERZ | Hellnaá | 64.06139 | −18.53400 | Pillow margin | Weichsel | This study | 3 | 29.09 | 0.65 | 2.25 | 4.06E+22 | 9.08E+20 |
| A31 | | ERZ | Hrútabjörg | 64.11031 | −18.46158 | Pillow margin | Weichsel | This study | 3 | 59.5 | 0.59 | 0.99 | 8.31E+22 | 8.24E+20 |
| A32 | | ERZ | NW of Grænifjallgardur | 64.10578 | −18.51542 | Pillow margin | | | | | | | | |
| A33 | | ERZ | Breidbak | 64.10594 | −18.56867 | Pillow margin | | | | | | | | |
| A34 | | ERZ | Hnausar | 64.08778 | −19.05417 | Pillow margin | Weichsel | This study | 8 | 30.67 | 1.11 | 3.61 | 4.28E+22 | 1.55E+21 |
| A35 | islhhj[b,c] | ERZ | Sigalda | 64.17217 | −19.13853 | Pillow margin | Weichsel | This study | 5 | 12.84 | 0.85 | 6.59 | 1.79E+22 | 1.19E+21 |
| A38 | ICE08R-25[b,c] | ERZ | Fellsendavatn | 64.18847 | −18.95700 | Pillow margin | | | | | | | | |
| HEL-2 | | WRZ | Helgafell | 64.01606 | −21.84244 | Pillow margin | Early Weichsel | *Saemundsson et al.* [2010] | 4 | 44.91 | 3.84 | 8.54 | 6.28E+22 | 5.37E+21 |
| HRA-1 | | WRZ | Hraunsvik | 63.85192 | −22.36867 | Pillow margin | Late Weichsel | *Saemundsson et al.* [2010] | | | | | | |
| HS92-15 | islhhc,k[b,c] | NRZ | Bláfjall | 65.42664 | −16.81561 | Pillow margin | ~14 ka | *Licciardi et al.* [2007] | 9 | 31.39 | 0.87 | 2.77 | 4.35E+22 | 1.21E+21 |
| HS92-16 | islhhl[b,c] | NRZ | Bláfjall | 65.42511 | −16.81606 | Pillow margin | ~14 ka | *Licciardi et al.* [2007] | 8 | 33.04 | 1.41 | 4.26 | 4.58E+22 | 1.95E+21 |
| ICE08R-07 | | WRZ | Stakur | 63.99644 | −21.88872 | Pillow margin | Early Weichsel | *Saemundsson et al.* [2010] | | | | | | |
| ICE08R-08 | A12[b,c] | ERZ | N- and S-Hágöngur | 64.56969 | −18.19967 | Pillow margin | | | | | | | | |
| ICE08R-09 | A13[b,c] | ERZ | Skerdingar-1 | 64.57161 | −18.07064 | Pillow margin | | | | | | | | |
| ICE08R-10 | A16[b,c] | ERZ | Bláfjall | 64.37169 | −18.24844 | Pillow margin | Weichsel | This study | | | | | | |
| ICE08R-12 | A18[b,c] | ERZ | Outcrop close to Dór | 64.38131 | −18.25056 | Pillow margin | | | | | | | | |
| ICE08R-13 | | ERZ | Bláfjall | 64.38956 | −18.22922 | Pillow margin | | | | | | | | |
| ICE08R-14 | A19[b,c] | ERZ | Ljósufjöll | 64.24325 | −18.58269 | Pillow margin | Weichsel | This study | 6 | 28.58 | 0.21 | 0.72 | 3.99E+22 | 2.93E+20 |
| ICE08R-15 | A20[b,c] | ERZ | Kambsfell | 64.82736 | −17.75550 | Pillow margin | Weichsel | This study | 3 | 33.06 | 1.9 | 5.75 | 4.60E+22 | 2.64E+21 |
| ICE08R-16 | A21[b,c] | ERZ | Gnjótsá | 64.82686 | −17.70228 | Pillow margin | Weichsel | This study | | | | | | |
| ICE08R-18 | A23[b,c] | ERZ | Gully near Valafell | 64.72367 | −17.72217 | Pillow margin | | | | | | | | |
| ICE08R-19 | A25[b,c] | ERZ | Svarthöfdi | 64.64253 | −17.86858 | Pillow margin | Weichsel | This study | | | | | | |
| ICE08R-20 | | ERZ | Fontur, craters | 64.25175 | −18.65233 | Pillow margin | Holocene | This study | | | | | | |
| ICE08R-23 | A36[b,c] | ERZ | Heljargjá | 64.32217 | −18.46050 | Pillow margin | Weichsel | This study | 3 | 36.1 | 3.77 | 10.44 | 5.04E+22 | 5.26E+21 |
| ICE08R-24 | A37[b,c] | ERZ | Miklagljúfur | 64.32050 | −18.43261 | Pillow margin | Weichsel | This study | 3 | 35.24 | 3.22 | 9.13 | 4.92E+22 | 4.49E+21 |



Journal of Geophysical Research: Solid Earth

10.1002/2014JB011828

AGU Journal of Geophysical Research: Solid Earth

10.1002/2014JB011828

**Table 1.** (continued)

| Site | Alternative Name | Region | Location | Latitude (°N) | Longitude (°E) | Sample Type | Age | Age Reference | *nn* | $B_F$ | $B_{F\sigma}$ | $B_{F\sigma}$ (%) | VADM | VADM$_\sigma$ |
|---|---|---|---|---|---|---|---|---|---|---|---|---|---|---|
| KVIH-1 | | NRZ | Kvihólafjöll | 65.84017 | −16.98622 | Pillow margin | Weichsel | This study | | | | | | |
| KVK117 | | NRZ | Lindafjöll | 64.86700 | −16.35000 | Pillow margin | Weichsel | This study | 7 | 25.94 | 1 | 3.87 | 3.61E+22 | 1.39E+21 |
| KVK118 | | NRZ | Kverkfjöll | 64.76700 | −16.63300 | Pillow margin | | | | | | | | |
| KVK119 | | NRZ | Kverkfjöll | 64.76700 | −16.50000 | Pillow margin | | | | | | | | |
| KVK77 | | NRZ | Kverkfjöll | 64.81667 | −16.48333 | Pillow margin | Weichsel | This study | 6 | 20.29 | 3.18 | 15.69 | 2.82E+22 | 4.42E+21 |
| LON-1 | | WRZ | Lönguhlídar | 63.97172 | −21.94506 | Pillow margin | Early Weichsel | *Saemundsson et al.* [2010] | | | | | | |
| MAE-1 | | WRZ | Mælifell | 64.10706 | −21.18192 | Pillow margin | Late Weichsel | *Saemundsson et al.* [2010] | | | | | | |
| NAL-213 | islhhh[b,c] | NRZ | Hvammsfjöll | 65.36383 | −16.67408 | Pillow margin | | | | | | | | |
| NAL-352 | | NRZ | Upptyppingar | | | Pillow margin | 48 ± 7 ka | *Guillou et al.* [2010] | | | | | | |
| NAL-356 | islhhd[b,c] | NRZ | Upptyppingar | 65.03300 | −16.23300 | Pillow margin | Weichsel | This study | 7 | 34.8 | 1.9 | 5.45 | 4.83E+22 | 2.64E+21 |
| NAL-440 | islhhe[b,c] | NRZ | Hrímalda | 64.92483 | −17.08558 | Pillow margin | Early Weichsel | This study | | | | | | |
| NAL-455 | islhhf[b,c] | NRZ | Kverkfjöll | 64.73842 | −16.62225 | Pillow margin | <0.78 Ma | *Jóhanesson and Saemundson* [2009] | 4 | 43.69 | 1.98 | 4.53 | 6.08E+22 | 2.76E+21 |
| NAL-460 | | NRZ | Theistareykir/Kistufjall | 65.87917 | −17.15561 | Pillow margin | Early Brunhes | *Saemundsson et al.* [2010] | 3 | 25.41 | 1.59 | 6.27 | 3.51E+22 | 2.20E+21 |
| NAL-500 | | NRZ | Gæsavatn | 64.78061 | −17.51131 | Pillow margin | Weichsel | This study | 4 | 30.79 | 1.41 | 4.59 | 4.28E+22 | 1.96E+21 |
| NAL-584 | islhhb[b,c] | NRZ | Dyngjufjöll Ytri | 65.16169 | −16.92431 | Pillow margin | Weichsel | This study | 6 | 35.3 | 3.55 | 10.07 | 4.90E+22 | 4.93E+21 |
| NAL-585 | | NRZ | Upptyppingar | 65.02797 | −16.22900 | Pillow margin | Weichsel | This study | | | | | | |
| NAL-595 | islhhg[b,c] | NRZ | Kistufell | 64.78994 | −17.18231 | Pillow margin | Weichsel | This study | 7 | 62.38 | 5.33 | 8.55 | 8.68E+22 | 7.41E+21 |
| NAL-611 | islhha,i[b,c] | NRZ | Kistufell | 64.79844 | −17.20033 | Pillow margin | Weichsel | This study | 14 | 57.62 | 4.59 | 7.97 | 8.02E+22 | 6.39E+21 |
| NAL-828 | | NRZ | Hrúthálsar | 64.32381 | −16.50278 | Pillow margin | | | | | | | | |
| NAL-837 | | NRZ | Kvihólafjöll | 65.84017 | −16.98622 | Pillow margin | Weichsel | This study | | | | | | |
| RET-1/VES-1 | | SIVZ | Réttarfell (Thórsmörk) | 63.67208 | −19.49233 | Pillow margin | | | | | | | | |
| REY-1 | | WRZ | Reykjanes viti | 63.81239 | −22.71367 | Pillow margin | 0–1.2 ka | *Saemundsson et al.* [2010] | | | | | | |
| THREN-1 | | WRZ | Threngsli | 64.00133 | −21.46261 | Pillow margin | Early Weichsel | *Saemundsson et al.* [2010] | | | | | | |
| VIF-1 | | WRZ | Vífilsfell | 64.04872 | −21.54022 | Pillow margin | Early Weichsel | *Saemundsson et al.* [2010] | | | | | | |

[a] Site column lists the primary site names used in this study, Alternative Names are corresponding labels for the same volcanic unit from other publications. Region names are the sampling areas shown in Figure 2. Age estimates are based on descriptions in section 3. The number of successful specimens per site is *nn*. $B_F$ is the average field strength, $B_{F\sigma}$ is the standard deviation of the average site estimate, and $B_{F\sigma}$ % is the percent difference. VADM and VADM$_\sigma$ are the average virtual axial dipole moment estimates and the standard deviation of the site mean, respectively. Common era abbreviated to C.E.

[b] This study.

[c] *Füri et al.* [2010].

[d] *Helgason and Duncan* [2001].

[e] *Stanton et al.* [2011].

[f] *Tanaka et al.* [2012].

[g] *Bergh and Sigvaldason* [1991].

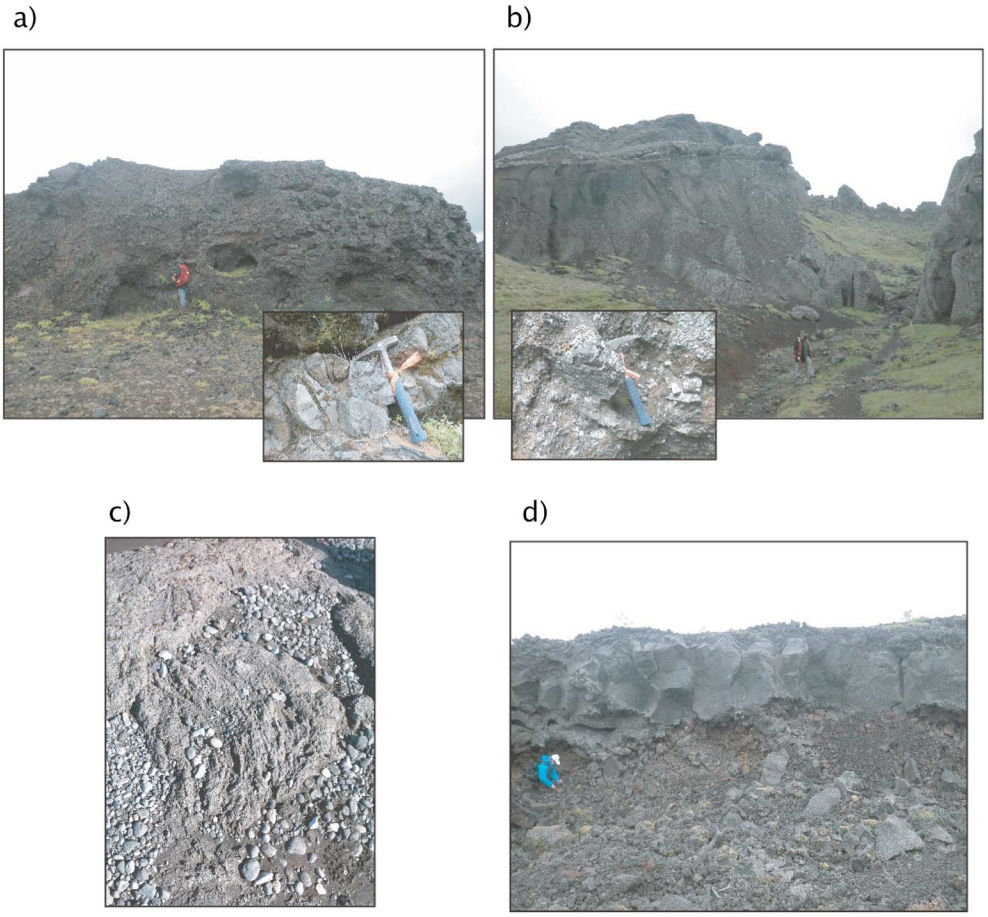


**Figure 3.** Photos of typical sample localities. (a) Pillow basalt outcrop (isl004). (b) Hyaloclastite sequence (isl009). (c) Pahoehoe flow top (isl048). (d) Subaerial lava flow bottom (isl066).

at the midpoint of a sequence of nine eruptive events. *Kristjánsson et al.* [1988] identified and numbered a total of 13 lava flows in the entire Núpakot sequence with Flow 1 located at the base. A single $^{40}K/^{39}Ar$ age determination, 0.78 ± 0.03 Ma [*McDougall et al.*, 1984], from the second eruptive unit above the base (Flow 2), confirms the geomagnetic polarity timescale age of the Núpakot section. In total, we collected samples from four sites from the Núpakot area, isl059–isl062.

### 3.3. Sida

This area in southeastern Iceland includes two main lithostratigraphic groups: subaerial lava flows and sediments of Holocene age and an older group of Pleistocene or late Pliocene hyaloclastites. *Jóhannesson and Saemundsson* [2009] map three voluminous Holocene lava flows that overlie the hyaloclastite group. Two lavas are historical, one from the 1783 C.E. Laki eruption and the second from the 934–940 C.E. Eldgjá event [*Thordarson and Hoskuldsson*, 2008]. The third lava is the Núpahraun flow, with an estimated $^{14}C$ age of 5.194 ± 0.04 ka [*Höskuldsson et al.*, 2012].

The older hyaloclastite sequence is nearly 700 m thick and consists of 14 basaltic volcanic units interbedded with minor lavas and sedimentary diamictites [*Bergh and Sigvaldason*, 1991; *Banik et al.*, 2014]. No radiometric dating is available for this group of lavas, but geologic maps [e.g., *Jóhannesson and Saemundsson*, 2009] identify the Sida group, and other areas of similar distance from the rift zone, as Pleistocene in age (0.78–3.3 Ma). *Saemundsson and Jóhannesson* [1980] collected paleodirectional information from Sida and determined a magnetostratigraphic age for the area that spans the Matuyama-Gauss polarity interval. In contrast, *Bergh and Sigvaldason* [1991] suggest that the fresh condition of the hyaloclastites indicates a relatively young age, perhaps not older than two or three glaciations or <0.3 Ma. Without absolute age controls, we follow the work of *Saemundsson and Jóhannesson* [1980] and adopt the Matuyama-Gauss polarity boundary age, 2.58 Ma [e.g., *Cande and Kent*, 1995], as an average age for the Sida group. This estimate is consistent with published

geologic maps [*Jóhannesson and Saemundsson*, 2009], but without radiometric dating the precise geochronology for the region is uncertain and additional work may be required in the future.

We sampled all three Holocene lavas in the Sida area (isl047–isl049 and isl052). Sites isl048 and isl052 were collected from the 1783 C.E. flow in two separate locations. Sites isl050, isl051, isl053–isl058, and isl063 were collected from the Matuyama/Gauss group.

### 3.4. Skaftafell

Skaftafell covers an area of about 300 $km^2$ and is located at the southern portion of the Vatnajökull ice cap, approximately 50 km east of the EVZ. The Vatnajökull glacier surrounds Skaftafell on all sides, except in the south where a low-angle coastal plain runs to the shoreline. Valley glaciers divide Skaftafell into four major sections: (from east to west) Svínafell, Hafrafell, Skaftafellsheidi, and Skaftafellsfjöll. *Helgason and Duncan* [2001] compiled a 2–3 km thick composite section of subaerial lava flows, pillow basalts, and hyaloclastite sequences and used magnetostratigraphy and $^{40}K/^{39}Ar$ geochronology to describe the complex geologic history of the area. Recent $^{40}Ar/^{39}Ar$ dates and detailed stratigraphy from Svínafell provide additional constraints on the volcanic history of that section [*Helgason and Duncan*, 2013]. At least 16 interglacial and glacial intervals are recorded in the volcanic strata over the last 5 Ma with an increasing frequency and intensity of glacial events since ~2.6 Ma. An exceptionally detailed geologic map [*Helgason*, 2007] accompanies the investigation of *Helgason and Duncan* [2001].

The Skaftafell sections are carved by millions of years of glacial activity and have steep valley faces that are accessible through stream channels and gullies. On average, the highest peaks for each section reach elevations of around 1000 m above sea level with varying degrees of slope. Thick lava flow sequences (~4.5 Ma) form the base of the Skaftafell area with alternating layers of interglacial/glacial volcanics stacked above. The youngest dated units at the top of each section are around 0.5 Ma. Most volcanic units are basaltic to intermediate in composition although young acidic formations are found at the top of Skaftafellsheidi and Skaftafellsfjöll. Field observations indicate these young acidic units are fed by an extensive dike system.

In total, we sampled 32 volcanic units in Skaftafell: six from Svínafell (isl015–isl020), 16 from Skaftafellsfjöll (isl021–isl036), and 10 from Hafrafell (isl037–ial046). At Skaftafellsheidi we walked up section SKH [see *Helgason*, 2007] but were unable to find any volcanic glass.

## 4. Methods

### 4.1. Paleointensity

Fresh-looking, glassy, and/or fine-grained specimens were picked and separated from larger hand samples in the laboratory. Specimens exhibiting any visible alteration features or superficial dirt were subjected to ultrasonic cleaning in order to remove material that could acquire a thermal magnetic signature during laboratory heatings. For the ultrasonic treatment, specimens were submerged in a 10% HCl solution in beakers which were then placed in an ultrasonic water bath for 15 min. The water bath was chilled to prevent the specimens from heating above 30°C and possibly acquiring a partial thermal remanent magnetization (pTRM). Following ultrasonic cleaning, all specimens with magnetic moments greater than $10^{-10}$ $Am^2$ were placed in labeled glass tubes for the paleointensity experiment.

We used the in-field/zero-field and zero-field/in-field (IZZI) version of the Thellier-Thellier paleointensity experiment [*Tauxe and Staudigel*, 2004] which was performed at Scripps Institution of Oceanography using custom-built ovens. A 2G Cryogenic Magnetometer was used to make natural remanent magnetization (NRM) and pTRM measurements at each laboratory heating step. Specimens were subject to a 35 μT or 20 μT field during in-field steps, and pTRM alteration checks were performed at every other temperature increment. IZZI experiments were carried out until at least 95% of the NRM was removed or when it was apparent that a specimen had altered during the heating process.

### 4.2. First-Order Reversal Curves

Select specimens were chosen for first-order reversal curve (FORC) analysis. All measurements were performed on the same specimens previously used in the paleointensity experiments. FORC experiments were performed on a Princeton Measurements Vibrating Sample Magnetometer at the Institute for Rock Magnetism at the University of Minnesota. FORC data were analyzed using *FORCInel* software of *Harrison and Feinberg* [2008]. Smoothing factors for each specimen were chosen based on the optimization routine in *FORCInel* with values ranging from 4 to 10.

**Table 2.** Selection Statistics at the Specimen and Sites Levels and Their Threshold Values[a]

| Statistics | Values |
|---|---|
| *Specimen* | |
| SCAT | - |
| FRAC | $\geq 0.78$ |
| Gap Max | $\geq 0.60$ |
| $\beta$ | $\leq 0.10$ |
| MAD | $\leq 5.0°$ |
| DANG | $\leq 10.0°$ |
| $\lvert\vec{k}'\rvert$ | $\leq 0.164$ |
| *Site* | |
| *nn* | $\geq 3$ |
| $B_\sigma$ | $\leq 4$ μT |
| $B_\sigma$ % | $\leq 10\%$ |

[a]See text for a brief definition of each criterion.

### 4.3. Selection Criteria

The Thellier GUI Auto Interpreter [*Shaar and Tauxe*, 2013] (part of the *PmagPy* software distribution available at http://earthref.org/PmagPy/cookbook) was used for paleointensity analysis. The Thellier GUI takes a uniform set of specimen and site level selection statistics and calculates objective interpretations of paleointensity data. Table 2 lists the selection criteria used in this study, and we provide brief descriptions of each statistic (for a complete description of all paleointensity statistics, see *Paterson et al.* [2014]). *SCAT* [*Shaar and Tauxe*, 2013] is a boolean statistic which uses the error on the best fit Arai plot [*Nagata et al.*, 1963] slope to test the degree of scatter over a range of NRM/TRM data points. *FRAC* [*Shaar and Tauxe*, 2013] is calculated from the NRM fraction of a select range of NRM/TRM data points on an Arai plot and is determined using the full difference vector sum calculation. *Gap Max* [*Shaar and Tauxe*, 2013] is the maximum gap between two NRM/TRM data points determined by vector arithmetic. Beta ($\beta$) [*Coe et al.*, 1978; *Tauxe and Staudigel*, 2004] measures the relative scatter around the best fit line in an Arai plot. It is defined as the ratio of the standard error of the slope to the absolute value of the slope. *DANG* [*Tauxe and Staudigel*, 2004] is the angular difference between the NRM components used in the best fit line and the angle that the line anchoring the center of mass makes with the origin. *MAD* [*Kirschvink*, 1980] is a measure of scatter about the best fit line through the NRM steps in an Arai plot. $\vec{k}'$ [*Paterson et al.*, 2014] is a measure of the degree of curvature in an Arai diagram between select temperature steps. A more curved arc has a higher value of $\vec{k}'$ and a perfectly straight line will have a $\vec{k}' = 0$. A threshold value of |0.164| has been shown to remove a low-field bias in sites with curved Arai plots [*Paterson*, 2011; *Cromwell et al.*, 2015].

Specimen and site level statistical requirements for this study were chosen based on the criteria of *Cromwell et al.* [2015]. In their paleointensity analysis of modern Hawaiian lava flows, *Cromwell et al.* [2015] determined that the expected magnetic field strength could be recovered to within 4% after applying the criteria listed in Table 2. These are appropriately strict for paleointensity investigations on glassy volcanics because the relatively high success rate of quenched material in Thellier-type experiments allows for more stringent analysis without significantly limiting the quantity of successful sites.

## 5. Representative Experimental Results

In this section, we examine the range of results from the IZZI paleointensity experiment and classify distributions of magnetic grain size and primary carriers for magnetic remanence. Figure 4 shows representative specimen behaviors that are most common in our Icelandic data set, including Arai plots that are nearly linear (Figure 4a), slightly curved (Figure 4d), or altered (Figure 4g).

Specimens isl007b4 and isl007b3 are from the same lava flow and show some variability of within-site experimental behavior (Figures 4a–4c and 4d–4f, respectively). The Arai plot for isl007b4 is very well behaved and passes all requirements while isl007b3 is slightly concave-up and fails the $\vec{k}'$ criterion. The estimated paleointensity from the curved specimen (isl007b3, 15.8 μT) is slightly lower than its well-behaved sister specimen (isl007b4, 16.9 μT) which is consistent with observations of *Paterson* [2011] and *Cromwell et al.* [2015]. Specimen isl009a2 (Figure 4g) alters at the 300°C heating step, causing a spiked, "hedgehog," behavior in the Arai plot and Zijderveld diagram at higher temperatures. The low-temperature component of this specimen is linear but does not pass the *FRAC* requirement of 0.78. In addition, the Zijderveld diagram shows that the same low-temperature component does not trend to the origin, resulting in a DANG value greater than 10°.

Hysteresis plots (Figures 4b, 4e, and 4h) and first-order reversal curve diagrams (Figures 4c, 4f, and 4i) suggest the presence of high-coercivity, single-domain magnetic carriers. Specimens isl007b4 and isl009a2 have

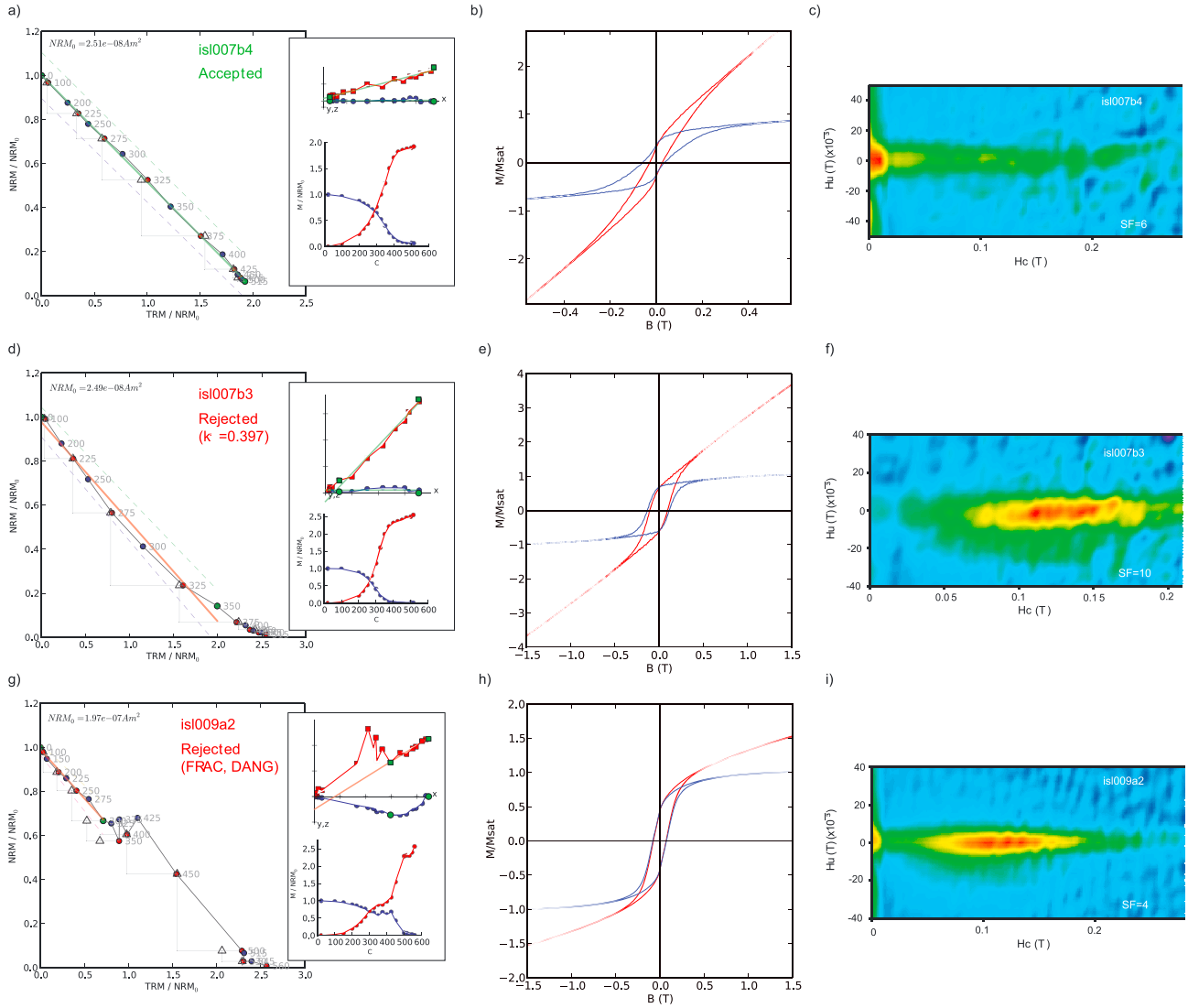


**Figure 4.** Representative paleointensity and rock magnetic results. (a, d, and g) Arai plots (with inset Zijderveld diagrams and NRM-decay/TRM-growth curves) are plotted. Temperature values for Arai plots are listed in degrees Celsius. pTRM checks are shown as open triangles, zero-field/in-field temperature steps shown as red dots, and in-field/zero-field steps shown in blue. The green line is the least squares component for selected temperature steps. *X* axes in the Zijderveld diagrams are rotated to the specimen declination. NRM-decay curves are shown in blue, and TRM-growth curves in red. (b, e, and h) Hysteresis loops show the raw hysteresis data in red, and the resulting loop after paramagnetic slope corrections in blue. (c, f, and i) First-order reversal curve (FORC) diagrams are plotted, and SF is the smoothing factor applied to each FORC.

magnetization of remanence to magnetization of saturation (Mr/Ms) ratios of 0.31 and 0.43, respectively, indicating a magnetic contribution from pseudo single-domain grains. Specimen isl007b3 has a high Mr/Ms ratio of 0.64 which has been previously observed in quenched seafloor basalts [*Gee and Kent*, 1995] and is shown to be the result of multiaxial single-domain carriers [*Tauxe et al.*, 2002; *Mitra et al.*, 2011; *Williams et al.*, 2011]. A recalculation of Mr/Ms ratios using the approach to saturation method of *Jackson and Solheid* [2010] resulted in slightly different Mr/Ms values for isl007b4 and isl009a2 (0.39 and 0.40, respectively). We found that specimen isl007b3 is best estimated by a linear fit; therefore, the approach to saturation method does not apply and the Mr/Ms value remains the same as above. FORC diagrams for each specimen show a distinct high-coercivity band along the *x* axis, indicative of single-domain magnetic material. This is to be expected considering the quenched volcanic material collected for this study is likely to be predominantly single domain. Each specimen also has some signal parallel to the Hu axis of the FORC diagram that could arise either from multidomain grains or from the thermal relaxation of superparamagnetic grains [*Pike et al.*, 2001]. Interestingly, the specimen with the best behaved Arai plot, isl007b4 (Figure 4a), has the greatest degree

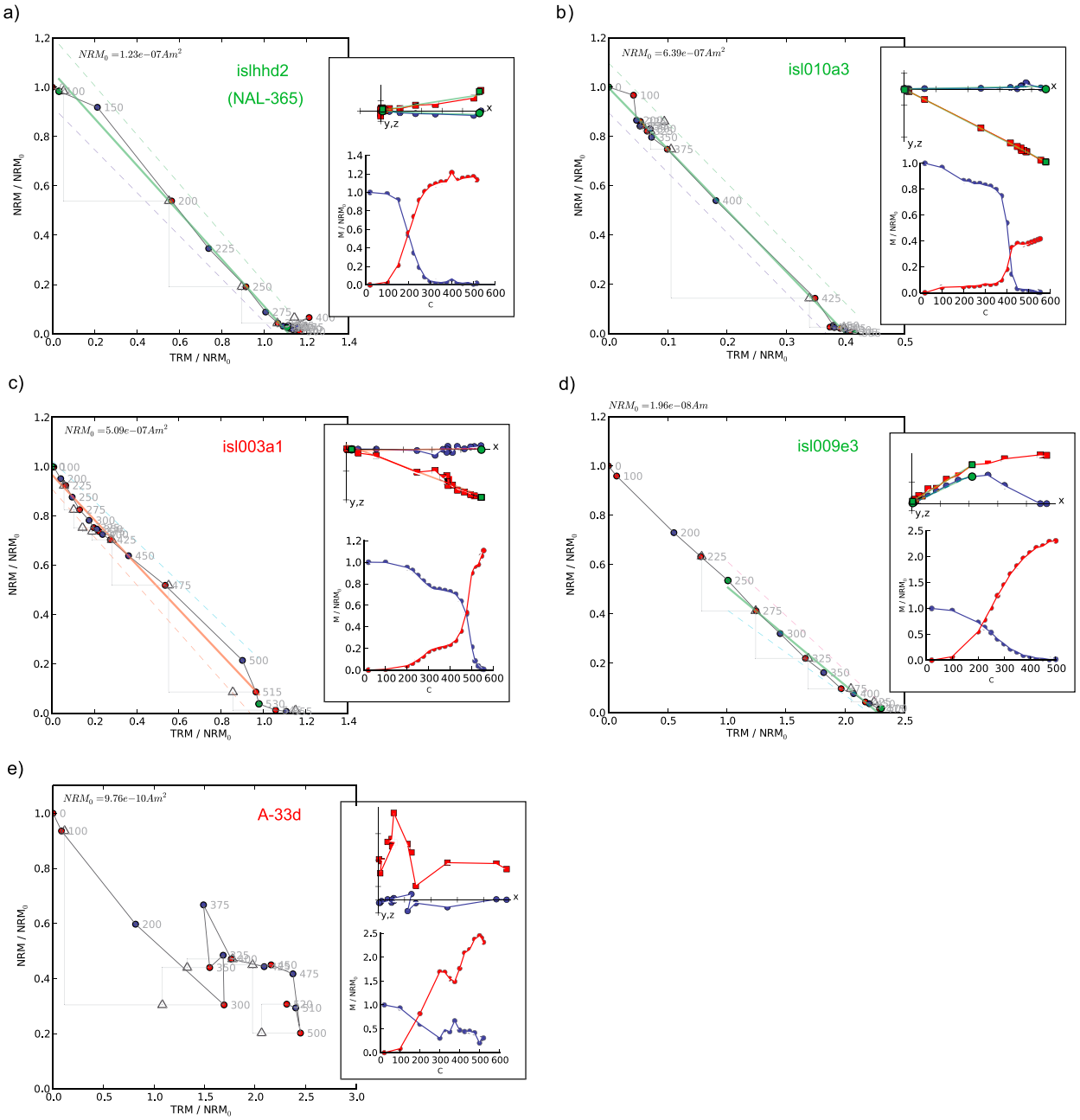


**Figure 5.** Representative experimental behaviors for (a, b, and d) accepted and (c and e) rejected specimens. Arai plots with inset Zijderveld diagrams and NRM-decay/TRM-growth curves are plotted for each specimen. The *x* axis of the Zijderveld diagrams is rotated to the specimen declination.

of low-coercivity behavior, suggesting that it is super paramagnetic rather than multidomain. Conversely, specimen isl009a2 has a beautiful FORC diagram but alters at a moderate temperature (~300°C). These observations suggest that room temperature FORC analyses alone are not necessarily good predictors of specimen behavior during paleointensity experiments.

The strict selection criteria we use in this study is the same as the requirements applied in *Cromwell et al.* [2015]. In that study, the authors determined through scanning electron microscope analysis that the primary magnetic carriers in their successful specimens were micrometer-scale, dendritic titanomagnetites. Similar observations of magnetic carriers were made by *Shaar and Feinberg* [2013]. Our successful specimens have very similar paleointensity and hysteresis behaviors, and it is likely that they are also dominated by single-domain-like dendritic titanomagnetites.

**Table 3.** Median Paleointensity Results for Grouped Sites[a]

| Group | Age Range (ka) | $N$ | $B_F$ (μT) | $B_{F\ mad}$ (μT) | VADM ($ZAm^2$) | $VADM_{mad}$ ($ZAm^2$) |
|---|---|---|---|---|---|---|
| Holocene | 0–11 | 4 | 55.8 | 15.6 | 78.1 | 22.0 |
| Late Weischel | 11–21 | 5 | 33.0 | 8.1 | 45.8 | 11.7 |
| Early Weischel | 21–110 | 4 | 37.7 | 4.9 | 52.7 | 7.0 |
| Weischel | 11–110 | 20 | 33.9 | 5.8 | 47.2 | 8.0 |
| Brunhes | 11–780 | 4 | 28.4 | 2.8 | 39.7 | 4.1 |
| Matuyama/Gauss | ~2580 | 6 | 28.7 | 6.7 | 40.2 | 9.4 |
| Gauss | 3200–3500 | 1 | 46.9 | 3.6 | 46.9 | 5.1 |
| All sites | 0–3500 | 44 | 34.9 | 9.8 | 48.6 | 13.9 |
| All Weischel | 11–110 | 29 | 34.8 | 6.4 | 48.3 | 9.2 |
| All Brunhes (ex-Hol) | 11–780 | 33 | 33.1 | 7.2 | 46.0 | 10.2 |
| All (ex-Holocene) | 11–3350 | 40 | 33.1 | 8.3 | 47.0 | 11.6 |

[a]Groups are based on stratigraphic age controls with approximate age ranges listed in kiloyears. The number of sites per group is $N$. $B_F$ and VADM are the median intensity and virtual axial dipole moment, $B_{F\ mad}$ and $VADM_{mad}$ are their respective median absolute deviations.

In Figure 4 we looked at experimental results that represent most specimens in our data set. We now characterize less common experimental behaviors (Figure 5) that are found in relatively few specimens but may pass our selection criteria to ensure that all results accurately reflect the ancient field strength and to justify our specimen selection process. Specimens with low blocking temperatures may pass our selection requirements (e.g., islhhd2, Figure 5a) but might be the result of a secondary chemical remanent magnetization (CRM) or a viscous remnant magnetization (VRM), in which case the resulting paleointensity estimate would not be representative of the ancient field when the lava was emplaced. Several lava flows have specimens with low blocking temperatures (like islhhd2), and when we compared those results to sister specimens with high-blocking temperatures, we found that paleointensities for both specimen types are comparable, indicating that the observed low blocking temperature is likely an original TRM. Specimen isl010a3 (Figure 5b) also has a small, low blocking temperature component (or "hump") in the NRM-decay/TRM-growth curve and is accepted by the ThellierGUI selection routine, but the bulk of the magnetization is carried by higher-temperature minerals. This low-temperature hump is likely a weathering feature due to the postemplacement production of goethite and subsequent magnetization in the direction of the ambient magnetic field. A different example of a "two-humped" demagnetization that is not accepted is shown in Figure 5c. In this case, the low blocking temperature component is between 300 and 400°C and is generally followed by signs of alteration during the heating experiment. These specimens often show different Arai slopes for each blocking temperature section, which results in the specimen failing SCAT. In some instances the change in slope is undetectable and the specimen will pass all selection statistics, suggesting that alteration is minimal and the specimen can be included in site mean analysis.

Specimen isl009e3 (Figure 5d) represents a case of a physical mechanism for a magnetic signature with two directional components. Generally, these types of behaviors fail the Thellier Gui selection process because the large FRAC requirement results in the MAD or DANG criteria exceeding their respective threshold values. Hyaloclastite sequences consist of volcaniclastic materials, like broken pillow fragments, that are deposited in layers. Prior to cooling completely through the magnetic blocking temperature, volcanic fragments may rotate, resulting in more than one directional component (see Zijderveld diagram in Figure 5d). For hyaloclastite specimens that exhibit a single rotation, we accept the high-blocking temperature component, regardless of FRAC, so long as that component passes all other selection statistics, and there is no sign of experimental alteration in the Arai plot.

Figure 5e (specimen A-33d) shows a small viscous remanent magnetization component at low temperatures, but the specimen alters at 300°C with no hope of passing any statistical requirements. Specimens exhibiting severe alteration were often removed from the paleointensity heating experiment prior to completion because they were sure to fail.

**Table 4.** Mean Paleointensity Results (μT) for the 1783 C.E. Laki Lava Flow, Sampled in This Study and by *Stanton et al.* [2011] and *Tanaka et al.* [2012]

| | Laki Flow (1783 C.E.) |
|---|---|
| This study | 45.12 ± 2.5, *nn* = 13 |
| *Stanton et al.* [2011] | 47.6 ± 5.1, *nn* = 6 |
| *Tanaka et al.* [2012] | 51.5 ± 1.7, *nn* = 4 |

## 6. Iceland Paleointensity Results

Forty-four sites (out of 129, ~35%) passed all site and specimen level selection criteria. Paleointensity results for each site are listed in Table 1, and median intensity estimates for different age groupings are listed in Table 3. We choose to calculate median values and median absolute deviation (*mad*) uncertainties, rather than mean values, because the median statistic is less affected by large outliers, and because we cannot assume that our intensity data are normally distributed, as intensities can only be positive and they are typically "long tailed" [*Ziegler et al.*, 2008].

Individual specimen results, statistics, and measurement level data from this study can be found in the MagIC database at http://earthref.org/MAGIC. Thirty-four sites are from the neovolcanic zone, and all but three are known to be Weichsel age (11–110 ka) or younger. Seven sites were collected in the Sida area, one of which, isl048/052, is the historic Laki eruption of 1783 C.E., and another, isl047, is the 5.194 ka Núpahraun lava flow [*Höskuldsson et al.*, 2012]. The other five Sida sites are estimated to be emplaced across the Matuyama-Gauss polarity boundary at 2.58 Ma [*Saemundsson and Jóhannesson*, 1980]. Three sites were successful from Skaftafell: isl020, isl041, and isl045. Site isl020 is Brunhes age [*Helgason and Duncan*, 2013], isl041 was emplaced between 3.20 and 3.35 Ma [*Helgason and Duncan*, 2001] and isl045 between 2.35 and 2.59 Ma [*Helgason and Duncan*, 2001]. No Núpakot area sites were successful.

One of our successful sites, the 1783 Laki lava flow (isl048/isl052) was also sampled by *Stanton et al.* [2011] and *Tanaka et al.* [2012] for paleointensity analysis. We collected material from the glassy bottom of this flow (e.g., Figure 3d), while the other researchers drilled standard paleomagnetic holes into the massive interior. *Stanton et al.* [2011] and *Tanaka et al.* [2012] both used the Coe variant of the Thellier-Thellier paleointensity method [*Coe*, 1967] with pTRM checks for alteration. *Tanaka et al.* [2012] also performed the Shaw intensity experiment [*Shaw*, 1974] on one sample from this site. Average results and uncertainties for all three studies are listed in Table 4. The mean intensity values for our study and *Stanton et al.* [2011] are within one standard deviation of each other, but the *Tanaka et al.* [2012] mean barely exceeds the 1$\sigma$ limit of our site. Our estimate has a within-site variance that is lower than *Stanton et al.* [2011] but slightly larger (1.2 μT) than *Tanaka et al.* [2012].

We plot the results for all 44 new Icelandic sites in Figure 6a, along with the median paleointensity value (34.9 μT). Four sites are Holocene age (open circles) with a median intensity of 55.8 ± 15.6 μT. This value is equivalent to the present-day Iceland field intensity of 52.5 μT (calculated from igrf.py in the *PmagPy*

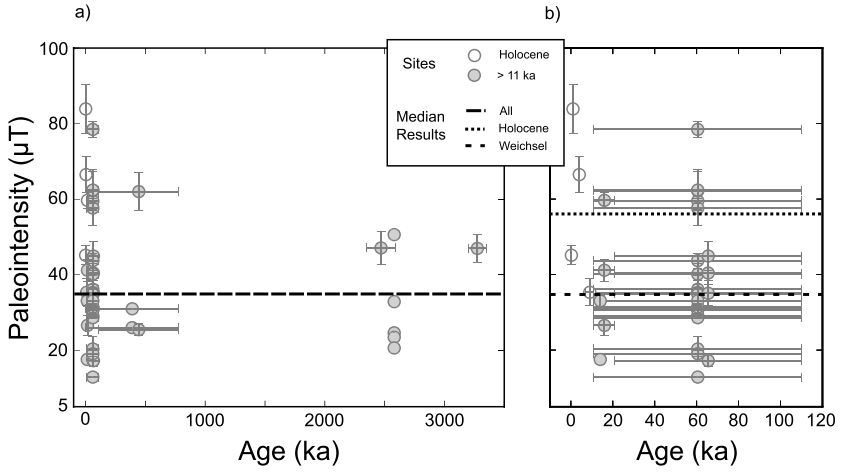


**Figure 6.** Paleointensity results (with 1$\sigma$ error bars) plotted with age for successful sites. Age estimates and uncertainties are listed in Table 1. (a) All sites. (b) Enlargement of Holocene and Weichsel-aged sites (0–110 ka). For clarity, any error bars smaller than the respective data point are not plotted.

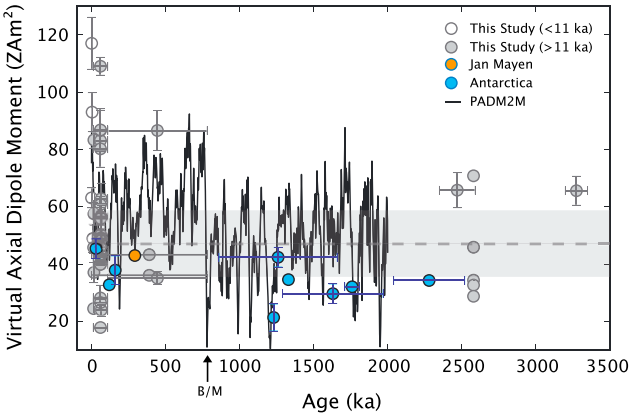


**Figure 7.** VADM site estimates for Holocene (open) and older (gray) Icelandic sites. High-latitude sites from Jan Mayen (orange, *Cromwell et al.* [2013]) and Antarctica (blue, *Lawrence et al.* [2009]) pass our strict selection criteria. PADM2M dipole moment model for 0–2 Ma [*Ziegler et al.*, 2011] shown in black. The dashed gray line is the median VADM for all Icelandic sites older than 11 ka (47.0 $ZAm^2$), and the shaded area reflects the median absolute deviation (±11.6 $ZAm^2$). The Brunhes/Matuyama boundary (B/M) is marked at 780 ka. For clarity, any error bars smaller than the respective data point are not plotted.

software distribution) and significantly higher than the median strength for all older sites (gray circles, $N$ = 40, 33.1 ± 8.3 μT). The Weichsel, Brunhes, and Matuyama/Gauss age intervals have equivalent median intensities of about 30 μT (Figure 6a and Table 3) and have similar site intensity distributions to each other.

Figure 6b is an enlargement of the Holocene and Weichsel age intervals (0–110 ka) showing the 33 youngest sites in Figure 6a (four Holocene and 29 Weichsel). Median intensities for each interval are shown as dashed lines, emphasizing the high Holocene field strength and similarity between Weichsel intensity and that of older age intervals in Figure 6a. Within the Weichsel period, we were able to stratigraphically constrain five sites as Late Weichsel (11–21 ka) and four sites as Early Weichsel (21–110 ka), which have median paleointensity estimates of 33.0 ± 8.1 μT and 37.7 ± 4.9 μT, respectively. The remaining 19 Weichsellian sites are undifferentiated within the Weichsel period and could potentially have ages anywhere within the time interval. These 19 sites have a median intensity of 33.9 ± 5.8 μT and span the range of field estimates for the early and late periods, suggesting that these 19 sites are temporally distributed throughout the entire Weichsel period.

## 7. Discussion

### 7.1. Long-Term Iceland Intensity

In Figure 7 we show the virtual axial dipole moments (VADMs) of our new Iceland sites (open and gray circles) and the PADM2M dipole moment model of *Ziegler et al.* [2011] (black line) which predicts the geomagnetic field strength for the last 2 Myr. The median field strength for our Iceland data older than 11 ka (47.0 $ZAm^2$) is plotted as a dashed gray line, and the *mad* uncertainty of the median (± 11.6 $ZAm^2$) is represented by the shaded area. Recalculated VADMs of published high-latitude sites from Jan Mayen (orange, *Cromwell et al.* [2013]) and McMurdo, Antarctica (blue, *Lawrence et al.* [2009]) are also plotted.

Brunhes age Iceland sites (11–780 ka, $N$ = 33) appear to agree with PADM2M, especially when taking into account the rather large age uncertainties for some lava flows. Median field strengths for both sets of data, however, show a substantially lower field in Iceland (46.0 ± 10.4 $ZAm^2$) compared to the PADM2M global model for the Brunhes (62.1 $ZAm^2$). Several Iceland sites of Weichsel age significantly underestimate PADM2M at the dipole low around 40 ka, suggesting that they might have been emplaced during the Laschamp excursion, and possibly influencing the lower overall field strength.

The median value of all non-Holocene paleointensity results (11 ka–3.3 Ma) are indistinguishable at the *mad* uncertainty level from the long-term geomagnetic field strength calculations of *Selkin and Tauxe* [2000] (46 $ZAm^2$, average of 0.3–300 Ma), *Juarez et al.* [1998] (42 $ZAm^2$, average of 0–160 Ma), and *Tauxe et al.* [2013] (42 $ZAm^2$, median of 0–200 Ma) but remains substantially lower than the long-term mean estimate of *Tauxe and Yamazaki* [2007] (63 $ZAm^2$, 0–170 Ma) and the median Brunhes value of PADM2M (62.1 $ZAm^2$). Long-term intensity calculations are based on compilations of global data and are dependent on the selection criteria used to select published results. *Juarez et al.* [1998], *Selkin and Tauxe* [2000], and *Tauxe et al.* [2013] based their estimates on data calculated using laboratory methods that checked for alteration, while *Tauxe and Yamazaki* [2007] and *Ziegler et al.* [2011] incorporated all available paleointensity data with no preselection requirements. The strict selection criteria used for our Icelandic data (including the use of pTRM checks) suggests that we have produced an accurate representation of field strength for the last few million years, and our

agreement with the time-averaged intensity estimates of *Juarez et al.* [1998], *Selkin and Tauxe* [2000], and *Tauxe et al.* [2013] indicates that those calculations are reasonable.

The accuracy of long-term paleointensity estimates with no data selection requirements remains unclear. *Cromwell et al.* [2015] addressed the accuracy of field estimates using bootstrap simulations of all available published data from the 1960 Kilauea lava flow on the Big Island of Hawaii. The distribution of published results from the 1960 flow are biased high, relative to the expected intensity value, and *Cromwell et al.* [2015] showed that this high bias will likely produce overestimates of the expected field, regardless of the number of samples used to calculate the mean value. Parametric bootstrap simulations of average field intensity at Hawaii, with full field vectors drawn from PSV model TK03 [*Tauxe and Kent*, 2004] and parameterized by the measured variability of 1960 flow results, result in an overestimate of the median TK03 intensity by 5–7 μT, or about 25% [*Cromwell et al.*, 2015]. These results suggest that global paleointensity estimates which include results from all types of laboratory methodologies (e.g., *Tauxe and Yamazaki* [2007] and *Ziegler et al.* [2011]) overestimate the geomagnetic field strength, perhaps by as much as 25%. If a ~60 $ZAm^2$ VADM is reduced by 25%, the resulting value would approximate the long-term field estimates calculated by *Juarez et al.* [1998], *Selkin and Tauxe* [2000], *Tauxe et al.* [2013], and our new Iceland results.

### 7.2. Volcanic Glass in Paleointensity Experiments

There is some debate in the paleomagnetic community as to whether volcanic glass of all ages are reliable recorders of magnetic field strength. Many investigations on glassy material from recent (< 200 ka) terrestrial [*Ferk and Leonhardt*, 2009; *Ferk et al.*, 2011; *Cromwell et al.*, 2015] and submarine lavas [*Carlut et al.*, 2000; *Pick and Tauxe*, 1993a; *Mejia et al.*, 1996; *Bowles et al.*, 2005, 2006] find that volcanic glass is well behaved during paleointensity experiments and consistently recovers the expected field strength when known. Studies on Cretaceous and Jurassic submarine basaltic glasses (SBGs) also find that these specimens yield successful paleointensity results [*Pick and Tauxe*, 1993b; *Tauxe and Staudigel*, 2004; *Tauxe et al.*, 2013]. There is some concern with these older samples that devitrification and relaxation of the glass structure over time may lead to the growth of new magnetite grains during laboratory heating experiments [*Smirnov and Tarduno*, 2003; *Riisager et al.*, 2003], which could affect intensity estimates. *Tauxe et al.* [2013], however, suggest that the growth of new magnetite [e.g., *Pick and Tauxe*, 1994; *Smirnov and Tarduno*, 2003] does not necessarily affect the outcome of a paleointensity experiment.

Thirty three of our 44 successful sites are younger than 200 ka and therefore unlikely to be affected by any new mineral growth at standard laboratory temperatures [*Bowles et al.*, 2011]. Eleven sites are determined to be at least Brunhes age, with the oldest site estimated to be ~3.35 Ma. Further investigation would be necessary to determine the effects, if any, of devitrification on our older sites. Investigations pertaining to the reliability of SBGs are substantially different from our study in terms of material and timescale. The studies referenced above use nearly perfect glass specimens taken from lavas emplaced ~ 100 Myr ago or synthetically produced in a laboratory. Our samples are not pure glass and likely contain measurable amounts of very fine grained, crystalline volcanic material. In addition, the timescales referenced for relaxation of the glass structure for devitrification (75–120 Ma [*Bowles et al.*, 2011]) are 1–2 orders of magnitude longer than our oldest specimens. How these differences might affect interpretations of devitrification and mineral growth is uncertain. The paleointensity results and experimental behaviors in our data set are consistent for all sites, regardless of age, and we believe we have recovered accurate and reasonable estimates of ancient magnetic field strength.

### 7.3. Reevaluation of Published Data

The strict selection criteria and experimental methodologies used in our study are not widely reproduced in the published literature, and there are currently no data from comparable experiments at high latitudes that have been filtered with such strict criteria. Accurate paleointensity results from both polar regions are required to sufficiently evaluate potential long-term nondipole structures in the Arctic or Antarctic. In their Antarctica paper, *Lawrence et al.* [2009] applied similar site and specimen level selection statistics to those in this paper, but their threshold values for each statistic were much looser, especially the required fraction of NRM used for each specimen ($f_{vds} \geq 0.30$ [see *Paterson et al.*, 2014]) which is less than half of our required FRAC value (≥ 0.78). Paleointensity estimates calculated from low percent fractions of NRM (< ~40 to 50%) are often incorrect and are usually biased to higher intensity values [*Chauvin et al.*, 2005] when authors select the steep, low-temperature component in the Arai plot. The error resulting from low NRM fractions is often the result of poorly behaved intensity data, where alteration or concave-up Arai plots can produce NRM/TRM diagrams with variable slopes. Accurate specimen intensity estimates depend on linear NRM/TRM plots which

should be constrained using objective selection statistics such as $\vec{k}'$ [*Paterson et al.*, 2014] or a combination of *SCAT* [*Shaar and Tauxe*, 2013] and a large NRM fraction. Mean site level paleointensity estimates will have greater uncertainties and could be systematically biased [e.g., *Chauvin et al.*, 2005; *Paterson*, 2011; *Cromwell et al.*, 2015] unless each specimen has a significant linear component and objective statistical controls.

We downloaded available high-latitude measurement level data from McMurdo, Antarctic [*Lawrence et al.*, 2009] and Jan Mayen, Norway [*Cromwell et al.*, 2013] from the MagIC database and applied our strict selection criteria to those data. From McMurdo, nine sites with radiometric ages younger than 5 Myr passed our specimen and site level requirements (from youngest to oldest: mc218, mc35, mc217, mc109, mc142, mc15, mc147, mc120, and mc117). One site from Jan Mayen also passed our criteria (JM012). Recalculated results from McMurdo (blue) and Jan Mayen (orange) are shown in Figure 7. The single Jan Mayen site and three McMurdo sites (mc218, mc35, and mc217) are of comparable age to the Weichsel and Brunhes age Iceland results, and McMurdo site mc117 was emplaced at approximately the same time as the Icelandic Matuyama/Gauss sites. The remaining five McMurdo results are from the Matuyama epoch and do not overlap with any northern high-latitude paleointensity data.

Similar field strength estimates should be expected from Jan Mayen and Iceland as they are separated by only ~500 km. The VADM of site JM012 is equivalent to several Brunhes age Iceland sites and approximates the PADM2M dipole moment model. This single-site comparison of high-latitude intensities supports some regional compatibility at Arctic latitudes, at least during the Brunhes epoch.

In their original analysis of Antarctic intensity, *Lawrence et al.* [2009] observed a median field strength of $38.0 \pm 12.0$ ZAm$^2$, from 41 sites, that was substantially lower than what is predicted for that location based on published data (e.g., Figure 1). Our strict reevaluation of the Antarctic collection produces an equivalent median field strength to *Lawrence et al.* [2009] (34.3 versus 38.0 ZAm$^2$, respectively), but the variance of accepted sites is greatly reduced, with *mad* uncertainty values of 3.6 ZAm$^2$ compared to 12.0 ZAm$^2$. Lower variance of the revised Antarctic data supports our use of strict analytical controls as a means to improve the precision of long-term paleointensity estimates.

Reinterpreted Antarctic VADMs are consistent with PADM2M and our Iceland results where they have similar ages; however, the overall median strength of the Antarctic data ($34.3 \pm 3.6$ ZAm$^2$) is lower than what we observe from Iceland sites older than 11 ka ($47.0 \pm 11.6$ ZAm$^2$). The Antarctic and Icelandic median values are distinct at the *mad* uncertainty level, and the relatively reduced Antarctic field strength could be due to incomplete temporal comparisons; there are five Matuyama-aged sites (mc109, mc142, mc15, mc147, and mc120) with no Icelandic counterparts. Both locations have average dipole moments that are lower than current values from low and mid latitudes, and both are similar to the long-term geomagnetic strength estimates of *Juarez et al.* [1998], *Selkin and Tauxe* [2000], and *Tauxe et al.* [2013]. These observations show comparable field behaviors at high latitudes that may represent a more accurate depiction of global field strength than do intensity data from lower latitudes, or it is possible that persistent nondipole field structures are found at high latitudes.

If we expand our discussion to include directional data from high latitudes, we see that there may be some significant differences between the Arctic and Antarctic. Relatively high dispersion of virtual geomagnetic poles (VGPs) from Antarctic lava flows [*Lawrence et al.*, 2009] suggest a field structure that may be unique to high southern latitudes. Arctic paleodirectional data ($N = 37$) for 0–2 [*Cromwell et al.*, 2013] show a reduced dispersion of VGPs relative to Antarctica ($N = 128$), consistent with observations of directional scatter between hemispheres for modern and recent [*Korte et al.*, 2011] field evaluations. Unfiltered VGP dispersion values from high northern latitudes [e.g., *Udagawa et al.*, 1999; *Cromwell et al.*, 2013] generally agree with TK03 [*Tauxe and Kent*, 2004] (which assumes a geocentric axial dipole field), while dispersion estimates from Antarctica exceed the PSV predictions of TK03. Arctic PSV analysis and the correlation of Icelandic paleointensities with some long-term global averages suggest that the geomagnetic field at high northern latitudes is consistent with a geocentric axial dipole for the last few million years. Time-averaged field structures in Antarctica, however, cannot be properly addressed at this time because there are still too few Antarctic paleointensity data that meet our selection criteria. The nine available results from McMurdo suggest that there may not be a significant difference between Antarctic and Arctic paleointensity, but the paucity of Southern Hemisphere data means that the possibility of hemispheric asymmetry between the two regions cannot be excluded.

## 8. Conclusions

We present a new collection of high-quality paleointensity results from Iceland. Thirty-seven sites were emplaced during the Brunhes epoch (0–780 ka) and seven sites between ~2.5 and 3.3 Ma. We collected rapidly cooled material from subaerial and subglacial volcanic units across Iceland and performed the IZZI-modified Thellier-Thellier experiment on all sites. The use of strict statistical criteria for site and specimen-level analyses produced paleointensity estimates with $1\sigma$ uncertainties not exceeding 4 μT or 10% of the site mean.

Four Holocene sites (<11 ka) have distinct intensities that approximate the present-day field in Iceland (52.5 μT or 80 $ZAm^2$) and are substantially higher than the median strength of all older sites. The 40 sites older than 11 ka have a median VADM of 47.0 ± 11.6 $ZAm^2$ (33.1 ± 8.3 μT) which is indistinguishable at the *mad* uncertainty level to long-term geomagnetic field strength calculations by *Selkin and Tauxe* [2000] (46 $ZAm^2$), and *Juarez et al.* [1998] and *Tauxe et al.* [2013] (42 $ZAm^2$, each). Agreement between our median Iceland field estimate (excluding Holocene data) and global average estimates suggests a GAD-like field intensity at high northern latitudes.

Reanalyzed high-latitude intensity results (using our strict selection criteria) from Antarctica ($N = 9$ [*Lawrence et al.*, 2009]) and Jan Mayen, Norway ($N = 1$ [*Cromwell et al.*, 2013]) are generally consistent with our Icelandic data, although the median Antarctic field strength is slightly lower. Recent paleosecular variation studies observe different VGP dispersion values between the Arctic and Antarctic, suggesting asymmetric field structures at high latitude. Our paleointensity observations are inconclusive as there are too few reliable intensity results from Antarctica to properly evaluate hemispheric differences.

**Acknowledgments**

We would like to thank Leo Kristjánsson and Johann Helgason for their scientific expertise and hospitality in planning and executing this project. Thank you to David Hilton for generously providing many of the Icelandic samples, Karl Grönvold for his work in the field, and Kristján Saemundsson for clarifying several lava flow emplacement ages. We thank the staff at Vatnajökull National Park and Simon Bergur Sigurgeirsson for allowing us to access and sample many of the localities. Thanks to Jason Steindorf and Jesse Vavrek for their hard work in the lab and Erol Cromwell for preparing many of the samples. Thanks to Ron Shaar, Hubert Staudigel, and Jeff Gee for discussions and comments leading to the success of this project. And thank you to Cathy Constable, David Hilton, Catherine Johnson, and Tom Levy for their constructive reviews. This research was partially supported by NSF EAR114840 and EAR1345003 to L.T. All measurement data and results can be found online in the MagIC database at http://earthref.org/MAGIC.

## References

Banik, T., P. Wallace, A. Höskuldsson, C. Miller, C. Bacon, and D. Furbish (2014), Magma-ice-sediment interactions and the origin of lava/hyaloclastite sequences in the Sída formation, South Iceland, *Bull. Volcanol.*, *76*, 785, doi:10.1007/s00445-013-0785-3.

Barry, P., D. Hilton, E. Füri, S. Halldórsson, and K. Grönvold (2014), Carbon isotope and abundance systematics of Icelandic geothermal gases, fluids and subglacial basalts with implications for mantle plume-related $CO_2$ fluxes, *Geochim. Cosmochim. Acta*, *134*, 74–99, doi:10.1016/j.gca.2014.02.038.

Bergh, S., and G. Sigvaldason (1991), Pleistocene mass-flow deposits of basaltic hyaloclastite on a shallow submarine shelf, South Iceland, *Bull. Volcanol.*, *53*, 597–611, doi:10.1007/BF00493688.

Bjarnason, I., and H. Schmeling (2009), The lithosphere and asthenosphere of the Iceland hotspot from surface waves, *Geophys. J. Int.*, *178*(1), 394–418, doi:10.1111/j.1365-246X.2009.04155.x.

Bowles, J., J. Gee, D. Kent, E. Bergmanis, and J. Sinton (2005), Cooling rate effects on paleointensity estimates in submarine basaltic glass and implications for dating young flows, *Geochem. Geophys. Geosyst.*, *6*, Q07002, doi:10.1029/2004GC000900.

Bowles, J., J. Gee, D. Kent, M. Perfit, S. Soule, and D. Fornari (2006), Paleointensity applications to timing and extent of eruptive activity, 9°–10° N East Pacific Rise, *Geochem. Geophys. Geosyst.*, *7*, Q06006, doi:10.1029/2005GC001141.

Bowles, J., J. Gee, K. Burgess, and R. Cooper (2011), Timing of magnetite formation in basaltic glass: Insights from synthetic analogs and relevance for geomagnetic paleointensity analysis, *Geochem. Geophys. Geosyst.*, *12*, Q02001, doi:10.1029/2010GC003404.

Brown, M., J. Shaw, and A. Goguitchaichvili (2006), Microwave palaeointensity from the R3-N3 geomagetic field reversal, *Geophys. J. Int.*, *167*, 53–69, doi:10.1111/j.1365-246X.2006.03034.x.

Camps, P., B. Singer, C. Carvallo, A. Goguitchaichvili, G. Fanjat, and B. Allen (2011), The Kamikatsura event and the Matuyama-Brunhes reversal recorded in lavas from Tjörnes Peninsula, northern Iceland, *Earth Planet. Sci. Lett.*, *310*(1–2), 33–44, doi:10.1016/j.epsl.2011.07.026.

Cande, S., and D. Kent (1995), Revised calibration of the geomagnetic polarity timescale for the late Cretaceous and Cenozoic, *J. Geophys. Res.*, *100*, 6093–6095, doi:10.1029/94JB03098.

Carlut, J., X. Quidelleur, V. Courtillot, and G. Boudon (2000), Paleomagnetic directions and K/Ar dating of 0 to 1 Ma lava flows from La Guadeloupe Island (French West Indias): Implications for time-averaged field models, *J. Geophys. Res.*, *105*(B1), 835–849, doi:10.1029/1999JB900238.

Chauvin, A., P. Roperch, and S. Levi (2005), Reliability of geomagnetic paleointensity data: The effects of the NRM fraction and concave-up behavior on paleointensity determinations by the Thellier method, *Phys. Earth Planet. Inter.*, *150*, 265–286.

Christensen, U., P. Olson, and G. Glatzmaier (1998), A dynamo model interpretation of the geomagnetic field structures, *Geophys. Res. Lett.*, *25*, 1565–1568.

Coe, R. (1967), Paleo-intensities of the Earth's magnetic field determined from Tertiary and Quaternary rocks, *J. Geophys. Res.*, *72*(12), 3247–3262.

Coe, R. S., S. Grommé, and E. A. Mankinen (1978), Geomagnetic paleointensities from radiocarbon-dated lava flows on Hawaii and the question of the Pacific nondipole low, *J. Geophys. Res.*, *83*, 1740–1756.

Cromwell, G., L. Tauxe, H. Staudigel, C. Constable, A. Koppers, and R.-B. Pedersen (2013), In search of long-term hemispheric asymmetry in the geomagnetic field: Results from high northern latitudes, *Geochem. Geophys. Geosyst.*, *14*, 3234–3249, doi:10.1002/ggge.20174.

Cromwell, G., L. Tauxe, H. Staudigel, and H. Ron (2015), Paleointensity estimates from historic and modern Hawaiian lava flows using glassy basalt as a primary source material, *Phys. Earth Planet. Inter.*, *241*, 44–56, doi:10.1016/j.pepi.2014.12.007.

Dunlop, D., and O. Özdemir (2001), Beyond Néel's theories: Thermal demagnetization of narrow-band partial thermoremanent magnetization, *Phys. Earth Planet. Inter.*, *126*, 43–57.

Einarsson, P. (2008), Plate boundaries, rifts and transformations in Iceland, *Jökull*, *58*, 35–58.

Ferk, A., and R. Leonhardt (2009), The Laschamp geomagnetic field excursion recorded in Icelandic lavas, *Phys. Earth Planet. Inter.*, *177*, 19–30.

Ferk, A., R. Leonhardt, K.-U. Hess, and D. Dingwell (2011), Paleointensities on 8 ka obsidan from Mayor Island, New Zealand, *Solid Earth*, *2*, 259–270, doi:10.5194/se-2-259-2011.

Füri, E., D. Hilton, S. Halldórsson, P. Barry, D. Hahm, T. Fischer, and K. Grönvold (2010), Apparent decoupling of the He and Ne isotope systematics of the Icelandic mantle: The role of He depletion, melt mixing, degassing fractionation and air interaction, *Geochim. Cosmochim. Acta*, *74*, 3307–3332, doi:10.1016/j.gca.2010.03.023.

Gee, J., and D. Kent (1995), Magnetic hysteresis in young mid-ocean ridge basalts: Dominant cubic anisotropy, *Geophys. Res. Lett.*, *22*(5), 551–554, doi:10.1029/95GL00263.

Geirsdóttir, A., and J. Eiríksson (1994), Growth of intermittent ice sheet in Iceland during the Late Pliocene and Early Pleistocene, *Quat. Res.*, *42*, 115–130.

Glatzmaier, A., R. S. Coe, L. Hongre, and P. Roberts (1999), The role of the Earth's mantle in controlling the frequency of geomagnetic reversals, *Nature*, *401*, 885–890.

Goguitchaichvili, A., M. Prevot, and P. Camps (1999), No evidence for strong fields during the R3-N3 Iceland geomagnetic reversal, *Earth Planet. Sci. Lett.*, *167*, 15–34.

Gubbins, D., A. Jones, and C. Finlay (2006), Fall in the Earth's magnetic field and implications for the geodynamo, *Science*, *312*, 900–902, doi:10.1126/science.1124855.

Guillou, H., B. van Vliet-Lanoë, A. Gudmundsson, and S. Nomade (2010), New unspiked K-Ar ages of Quaternary sub-glacial and sub-aerial volcanic activity in Iceland, *Quat. Geochronol.*, *5*, 10–19, doi:10.1016/j.quageo.2009.08.007.

Harrison, R., and J. Feinberg (2008), FORCinel: An improved algorithm for calculating first-order reversal curve distributions using locally weighted regression smoothing, *Geochem. Geophys. Geosyst.*, *9*, Q05016, doi:10.1029/2008GC001987.

Helgason, J. (2007), Skaftafell bedrock geology, 1:25.000. *Jóhann Helgason, Jardfraedistofan Ekra*.

Helgason, J., and R. Duncan (2001), Glacial-interglacial history of the Skaftafell region, southeast Iceland, 0–5 Ma, *Geology*, *29*(2), 179–182, doi:10.1130/0091-7613(2001)029<0179:GIHOTS>2.0.CO;2.

Helgason, J., and R. Duncan (2013), Stratigraphy, $^{40}$Ar-$^{39}$Ar dating and erosional history of Svínafell, SE-Iceland, *Jökull*, *63*, 33–54.

Herrero-Bervera, E., and J. P. Valet (2009), Testing determinations of absolute paleointensity from the 1955 and 1960 Hawaiian flows, *Earth Planet. Sci. Lett.*, *287*, 420–433.

Hjartarson, A. (1994), Environmental changes in Iceland following the Great Thjórsá Lava Eruption 7800 $^{14}$C years BP, in *Environmental Change in Iceland*, edited by J. Stötter and F. Wilhelm, pp. 147–155, Münchener Geographische Abhandlungen, Reihe B Munchen.

Höskuldsson, A., G. Larsen, B. Óladóttir, and O. Sigmarsson (2012), *Aldur Núpahrauns í Vestur-Skaftafellssýslu (in Icelandic)*, Geol. Soc. of Iceland, Spring Meeting, Reykjavik.

Hulot, G., C. Eymin, B. Langlais, M. Mandea, and N. Olsen (2002), Small-scale structure of the geodynamo inferred from Oersted and Magsat satellite data, *Nature*, *416*(6881), 620–623, doi:10.1038/416620a.

Jackson, A., A. R. T. Jonkers, and M. R. Walker (2000), Four centuries of geomagnetic secular variation from historical records, *Philos. Trans. R. Soc. London, Ser. A*, *358*(1768), 957–990.

Jackson, M., and P. Solheid (2010), On the quantitative analysis and evaluation of magnetic hysteresis data, *Geochem. Geophys. Geosyst.*, *11*, Q04Z15, doi:10.1029/2009GC002932.

Jakobsson, S., K. Jonasson, and I. Sigurdsson (2008), The three igneous rock series of Iceland, *Jökull*, *58*, 117–138.

Jicha, B., L. Kristjánsson, M. Brown, B. Singer, B. Beard, and C. Johnson (2011), New age for the Skálamaelifell excursion and identification of a global geomagnetic event in the late Brunhes chron, *Earth Planet. Sci. Lett.*, *310*, 509–517, doi:10.1016/j.epsl.2011.08.007.

Jóhannesson, H. (1983), Fródleiksmolar um Grænalón og nágrenni (in Icelandic), *Náttúrufrædingurinn*, *52*, 86–101.

Jóhannesson, H. (1985), Um endasleppu hraunin undir Eyjafjöllum og jökla sídasta jökulskeids (in Icelandic), *Jökull*, *35*, 51–60.

Jóhannesson, H., and S. Einarsson (1988), Krísuvíkureldar I: Aldur Ögmundarhrauns og midaldalagsins (The Krýsuvík fires I: Age of the Ögmundarhraun lava and the Medieval tephra layer), *Jökull*, *38*, 103–109.

Jóhannesson, H., and K. Saemundsson (2009), *Geological Map of Iceland. 1:600 000. Bedrock Geology,* 1st ed., Icelandic Institute of Natural History, Reykjavik.

Johnson, C. L., and C. Constable (1996), Palaeosecular variation recorded by lava flows over the past five million years, *Philos. Trans. R. Soc. London, Ser. A*, *354*, 89–141, doi:10.1098/rsta.1996.0004.

Jónsson, J. (1974), Óbrinnishólar (In Icelandic), *Náttúrufrædingurinn*, *44*, 109–119.

Juarez, M., L. Tauxe, J. Gee, and T. Pick (1998), The intensity of the Earth's magnetic field over the past 160 million years, *Nature*, *394*(6696), 878–881.

Kelly, P., and D. Gubbins (1997), The geomagnetic field over the past 5 million years, *Geophys. J. Int.*, *128*, 315–330, doi:10.1111/j.1365-246X.1997.tb01557.x.

Kent, D., and J. Gee (1996), Magnetic alteration of zero-age oceanic basalt, *Geology*, *24*, 703–706, doi:10.1130/0091-7613(1996)024<0703:MAOZAO>2.3.CO;2.

Kirschvink, J. L. (1980), The least-squares line and plane and the analysis of paleomagnetic data, *Geophys. J. R. Astron. Soc.*, *62*, 699–718, doi:10.1111/j.1365246X.1980.tb02601.x.

Korte, M., C. Constable, F. Donadini, and R. Holme (2011), Reconstructing the Holocene geomagnetic field, *Earth Planet. Sci. Lett.*, *312*, 497–505, doi:10.1016/j.epsl.2011.10.031.

Kristjánsson, L. (2010), Paleomagnetic observations at three locations in the Pleistocene lava sequences of southwest and south Iceland, *Jökull*, *60*, 149–164.

Kristjánsson, L. (2013), Analyses of primary remanence vector data from a large collection of lava flows: Towards improved methodology in paleo-geomagnetism, *Stud. Geophys. Geod.*, *57*(4), 543–564, doi:10.1007/s11200-012-0480-4.

Kristjánsson, L., I. Fridleifsson, and N. Watkins (1980), Stratigraphy and paleomagnetism of the Esja, Eyrarfjall and Akrafjall Mountains, SW-Iceland, *J. Geophys.*, *47*, 31–42.

Kristjánsson, L., H. Jóhannesson, J. Eiríksson, and A. Gudmundsson (1988), Brunhes-Matuyama paleomagnetism in three lava sections in Iceland, *Can. J. Earth Sci.*, *25*, 215–225, doi:10.1139/e88-024.

Kristjánsson, L., R. Duncan, and A. Gudmundsson (1998), Stratigraphy, palaeomagnetism and age of volcanics in the upper regions of Thjórsárdalur valley, central southern Iceland, *Boreas*, *27*, 1–13, doi:10.1111/j.1502-3885.1998.tb00863.x.

Lawley, E. (1970), The intensity of the geomagnetic field in Iceland during Neogene polarity transitions and systematic deviations, *Earth Planet. Sci. Lett.*, *10*, 145–149.

Lawrence, K. P., L. Tauxe, H. Staudigel, C. Constable, A. Koppers, W. C. McIntosh, and C. L. Johnson (2009), Paleomagnetic field properties near the southern hemisphere tangent cylinder, *Geochem. Geophys. Geosyst.*, *10*, Q01005, doi:10.1029/2008GC00207.

Levi, S., H. Audunsson, R. A. Duncan, L. Kristjansson, P. Y. Gillot, and S. Jakobsson (1990), Late Pleistocene geomagnetic excursion in Icelandic lavas: Confirmation of the Laschamp excursion, *Earth Planet. Sci. Lett.*, *96*, 443–457.

Licciardi, J., M. Kurz, and J. Curtice (2007), Glacial and volcanic history of Icelandic table mountains from cosmogenic He-3 exposure ages, *Quat. Sci. Rev.*, *26*(11–12), 1529–1546, doi:10.1016/j.quascirev.2007.02.016.

Love, J., and C. Constable (2003), Gaussian statistics for palaeomagnetic vectors, *Geophys. J. Int.*, *152*, 515–565, doi:10.1046/j.1365-246X.2003.01858.x.

Macpherson, C., D. Hilton, J. Day, D. Lowry, and K. Grönvold (2005), High-$^3$He/$^4$He, depleted mantle and low-$\delta^{18}$O, recycled oceanic lithosphere in the source of central Iceland magmatism, *Earth Planet. Sci. Lett.*, *233*(3–4), 411–427, doi:10.1016/j.epsl.2005.02.037.

Marshall, M., A. Chauvin, and N. Bonhommet (1988), Preliminary paleointensity measurements and detailed magnetic analyses of basalts from the Skálamaelifell excursion, Southwest Iceland, *J. Geophys. Res.*, *93*, 11,681–11,698, doi:10.1029/JB093iB10p11681.

McDougall, I., K. Saemundsson, H. Johannesson, N. Watkins, and L. Kristjánsson (1977), Extension of the geomagnetic polarity time scale to 5.5 m.y.: K-Ar dating, geological and paleomagnetic study of a 3,500-m lava succession in western Iceland, *Bull. Geol. Soc. Am.*, *88*, 1–15, doi:10.1130/0016-7606(1977)88<1:EOTGPT>2.0.CO;2.

McDougall, I., L. Kristjánsson, and K. Saemundsson (1984), Magnetostratigraphy and geochronology of northwest Iceland, *J. Geophys. Res.*, *89*, 7029–7060, doi:10.1029/JB089iB08p07029.

Mejia, V., N. Opdyke, and M. Perfit (1996), Paleomagnetic field intensity recorded in submarine basaltic glass from the East Pacific Rise, the last 69 ka, *Geophys. Res. Lett.*, *23*(5), 475–478, doi:10.1029/96GL00018.

Mitra, R., L. Tauxe, and J. Gee (2011), Detecting uniaxial single domain grains with a modified IRM technique, *Geophys. J. Int.*, *187*, 1250–1258, doi:10.1111/j.1365-246X.2011.05224.x.

Nagata, T., Y. Arai, and K. Momose (1963), Secular variation of the geomagnetic total force during the last 5000 years, *J. Geophys. Res.*, *68*, 5277–5282.

Olson, P., and J. Aurnou (1999), A polar vortex in the Earth's core, *Nature*, *402*(6758), 170–173, doi:10.1038/46017.

Paterson, G. (2011), A simple test for the presence of multidomain behavior during paleointensity experiments, *J. Geophys. Res.*, *116*, B10104, doi:10.1029/2011JB008369.

Paterson, G., L. Tauxe, A. Biggin, R. Shaar, and L. Jonestrask (2014), On improving the selection of Thellier-type paleointensity data, *Geochem. Geophys. Geosyst.*, *15*, 1180–1192, doi:10.1002/2013GC005135.

Pick, T., and L. Tauxe (1993a), Holocene paleointensities: Thellier experiments on submarine basaltic glass from the East Pacific Rise, *J. Geophys. Res.*, *98*(B10), 17,949–17,964, doi:10.1038/366238a0.

Pick, T., and L. Tauxe (1993b), Geomagnetic palaeointensities during the Cretaceous normal superchron measured using submarine basaltic glass, *Nature*, *366*, 238–242, doi:10.1038/366238a0.

Pick, T., and L. Tauxe (1994), Characteristics of magnetite in submarine basaltic glass, *Geophys. J. Int.*, *119*(1), 116–128, doi:10.1111/j.1365-246X.1994.tb00917.x.

Pike, C., A. Roberts, M. Dekkers, and K. Verosub (2001), An investigation of multi-domain hysteresis using FORC diagrams, *Phys. Earth Planet. Inter.*, *126*(1–2), 11–25, doi:10.1016/S0031-9201(01)00241-2.

Riisager, P., J. Riisager, X. Zhao, and R. Coe (2003), Cretaceous geomagnetic paleointensities: Thellier experiments on pillow lavas and submarine basaltic glass from the Ontong Java Plateau, *Geochem. Geophys. Geosyst.*, *4*(12), 8803, doi:10.1029/2003GC000611.

Roberts, N., and J. Shaw (1984), The relationship between the magnitude and direction of the geomagnetic field during the Late Tertiary in Eastern Iceland, *Geophys. J. R. Astron. Soc.*, *76*, 637–651.

Saemundsson, K., and H. Jóhannesson (1980), *Jardfrædirannsóknir á Fljótshverfis- og Sídumannaafréttum (In Icelandic)*, Geol. Soc. of Iceland Meeting, Reykjavík.

Saemundsson, K., and H. Noll (1974), K/Ar ages of rocks from Husafell, Western Iceland and the development of the Husafell central volcano, *Jökull*, *24*, 40–59.

Saemundsson, K., H. Jóhannesson, A. Hjartarson, S. Kristinsson, and M. Sigurgeirsson (2010), *Geological Map of Southwest Iceland, 1:100 000*, Iceland GeoSurvey, Reykjavik.

Schweitzer, C., and H. Soffel (1980), Palaeointensity measurements on postglacial lavas from Iceland, *J. Geophys.*, *47*, 57–60.

Selkin, P., and L. Tauxe (2000), Long-term variations in palaeointensity, *Philos. Trans. R. Soc. London, Ser. A*, *358*, 1065–1088.

Senanayake, W., M. McElhinny, and P. McFadden (1982), Comparison between the Thelliers' and Shaw's palaeointensity methods using basalts less than 5 million years old, *J. Geomagn. Geoelec.*, *34*, 141–161.

Shaar, R., and J. Feinberg (2013), Rock magnetic properties of dendrites: Insights from MFM imaging and implications for paleomagnetic studies, *Geochem. Geophys. Geosyst.*, *14*, 407–421, doi:10.1002/ggge.20053.

Shaar, R., and L. Tauxe (2013), Thellier Gui: An integrated tool for analyzing data from Thellier-type experiments, *Geochem. Geophys. Geosyst.*, *14*, 677–692, doi:10.1002/ggge.20062.

Shaw, J. (1974), A new method of determining the magnitude of the paleomagnetic field application to five historic lavas and five archeological samples, *Geophys. J. R. Astron. Soc.*, *39*, 133–141.

Shaw, J. (1975), Strong geomagnetic fields during a single Icelandic polarity transition, *Geophys. J. R. Astron. Soc.*, *40*, 345–350, doi:10.1111/j.1365-246X.1975.tb04136.x.

Sinton, J., K. Grönvold, and K. Saemundsson (2005), Postglacial eruptive history of the Western Volcanic Zone, Iceland, *Geochem. Geophys. Geosyst.*, *6*, Q12009, doi:10.1029/2005GC001021.

Smirnov, A., and J. Tarduno (2003), Magnetic hysteresis monitoring of Cretaceous submarine basaltic glass during Thellier paleointensity experiments: Evidence for alteration and attendant low field bias, *Earth Planet. Sci. Lett.*, *206*, 571–585, doi:10.1016/S0012-821X(02)01123-8.

Stanton, T., P. Riisager, M. Knudsen, and T. Thordarson (2011), New palaeointensity data from Holocene Icelandic lavas, *Phys. Earth Planet. Inter.*, *186*, 1–10, doi:10.1016/j.pepi.2011.01.006.

Tanaka, H., M. Kono, and H. Uchimura (1995a), Some global features of palaeointensity in geological time, *Geophys. J. Int.*, *120*, 97–102, doi:10.1111/j.1365-246X.1995.tb05913.x.

Tanaka, H., M. Kono, and S. Kaneko (1995b), Paleosecular variation of direction and intensity from two Pliocene-Pleistocene lava sections in southwestern Iceland, *J. Geomagn. Geoelec.*, *47*, 89–102.

Tanaka, H., Y. Hashimoto, and N. Morita (2012), Palaeointensity determinations from historical and Holocene basalt lavas in Iceland, *Geophys. J. Int.*, *189*(2), 833–845, doi:10.1111/j.1365-246X.2012.05412.x.

Tauxe, L., and D. V. Kent (2004), A simplified statistical model for the geomagnetic field and the detection of shallow bias in paleomagnetic inclinations: Was the ancient magnetic field dipolar?, in *Timescales of the Paleomagnetic Field*, vol. 145, edited by J. E. T. Channell et al., pp. 101–116, AGU, Washington, D. C.

Tauxe, L., and H. Staudigel (2004), Strength of the geomagnetic field in the Cretaceous Normal Superchron: New data from submarine basaltic glass of the Troodos Ophiolite, *Geochem. Geophys. Geosyst.*, *5*, Q02H06, doi:10.1029/2003GC000635.

Tauxe, L., and T. Yamazaki (2007), Paleointensities, in *Geomagnetism, Treatise on Geophysics*, vol. 5, edited by L. Tauxe and T. Yamazaki, pp. 509–563, Elsevier, Amsterdam.

Tauxe, L., H. Bertram, and C. Seberino (2002), Physical interpretation of hysteresis loops: Micromagnetic modeling of fine particle magnetite, *Geochem. Geophys. Geosyst.*, *3*(10), 1055, doi:10.1029/2001GC000241.

Tauxe, L., J. Gee, M. Steiner, and H. Staudigel (2013), Paleointensity results from the Jurassic: New constraints from submarine basaltic glasses of ODP Site 801C, *Geochem. Geophys. Geosyst.*, *14*, 4718–4733, doi:10.1002/ggge/20282.

Thordarson, T., and A. Hoskuldsson (2008), Postglacial volcanism in Iceland, *Jökull*, *58*, 197–228.

Udagawa, S., H. Kitagawa, A. Gudmundsson, O. Hiroi, T. Koyaguchi, H. Tanaka, L. Kristjansson, and M. Kono (1999), Age and magnetism of lavas in Jökuldalur area, Eastern Iceland: Gilsá event revisited, *Phys. Earth Planet. Inter.*, *115*, 147–171, doi:10.1016/S0031-9201(99)00073-4.

Walker, G. (1959), Geology of the Reydarfjördur area, eastern Iceland, *Q. J. Geol. Soc. London*, *114*, 367–391.

Watkins, N., and G. Walker (1977), Magnetostratigraphy of eastern Iceland, *Am. J. Sci.*, *277*, 513–584.

Williams, W., A. Muxworthy, and M. Evans (2011), A micromagnetic investigation of magnetite grains in the form of Platonic polyhedra with surface roughness, *Geochem. Geophys. Geosyst.*, *12*, Q10Z31, doi:10.1029/2011GC003560.

Ziegler, L., C. Constable, and C. Johnson (2008), Testing the robustness and limitations of 0–1 Ma absolute paleointensity data, *Phys. Earth Planet. Inter.*, *170*(1–2), 34–45, doi:10.1016/j.pepi.2008.07.027.

Ziegler, L., C. Constable, C. L. Johnson, and L. Tauxe (2011), PADM2M: A penalized maximum likelihood model of the 0–2 Ma palaeomagnetic axial dipole moment, *Geophys. J. Int.*, *184*, 1069–1089, doi:10.1111/j.1365-246X.2010.04905.x.